Glass-forming ability and structural features of melt-quenched and gel-derived SiO2-TiO2 glasses

Alessio Zandonà, Erwan Chesneau, Gundula Helsch, Aurélien Canizarès, Joachim Deubener, Valérie Montouillout, Franck Fayon, Mathieu Allix

▶ **To cite this version:**

Alessio Zandonà, Erwan Chesneau, Gundula Helsch, Aurélien Canizarès, Joachim Deubener, et al.. Glass-forming ability and structural features of melt-quenched and gel-derived SiO2-TiO2 glasses. Journal of Non-Crystalline Solids, 2022, 598, pp.121967. 10.1016/j.jnoncrysol.2022.121967 . hal-03874481

HAL Id: hal-03874481
https://hal.science/hal-03874481v1

Submitted on 28 Nov 2022

HAL is a multi-disciplinary open access archive for the deposit and dissemination of scientific research documents, whether they are published or not. The documents may come from teaching and research institutions in France or abroad, or from public or private research centers.

L'archive ouverte pluridisciplinaire **HAL**, est destinée au dépôt et à la diffusion de documents scientifiques de niveau recherche, publiés ou non, émanant des établissements d'enseignement et de recherche français ou étrangers, des laboratoires publics ou privés.

Glass-forming ability and structural features of melt-quenched and gel-derived SiO_2-TiO_2 glasses

Alessio Zandonà[a]*, Erwan Chesneau[a], Gundula Helsch[b], Aurélien Canizarès[a], Joachim Deubener[b], Valérie Montouillout[a], Franck Fayon[a], Mathieu Allix[a]

[a] CNRS, CEMHTI UPR3079, Univ. Orléans, F-45071 Orléans, France

[b] Clausthal University of Technology, Institute of Non-Metallic Materials, 38678 Clausthal-Zellerfeld, Germany

Abstract

SiO_2-TiO_2 glasses produced by aerodynamic levitation coupled to laser heating or by sol-gel spray-drying were compared to highlight their structural differences. Glass formation was possible by melt-quenching up to 10 mol% TiO_2, while higher contents led to devitrification. Raman spectroscopy and solid-state ^{17}O and ^{29}Si **magic-angle-spinning nuclear magnetic resonance** confirmed the clear emergence of Ti-O-Si bonds and a tetrahedral oxygen coordination of Ti^{4+} leading to full network connectivity, as also substantiated by the synthesis of TiO_2-doped cristobalite. In gel-derived glasses, water content induced partial network depolymerization, thereby enhancing the solubility of TiO_2 in the hydrous silicate matrix. However, full dehydration during heating proved challenging due to a competing tendency towards devitrification: the glass-forming range in the anhydrous binary SiO_2-TiO_2 system does not therefore appear to be significantly enlarged by the sol-gel synthesis route.

Keywords: glass-forming ability, Raman spectroscopy, solid-state NMR, titania silica glasses, cristobalite

***Corresponding author:** alessio.zandona@cnrs-orleans.fr

1. Introduction

The incorporation of Ti^{4+} in silicate melts and glasses has attracted an unceasing research interest in both geoscience and materials science. TiO_2 is indeed a frequent secondary component of terrestrial and lunar rocks and has been evaluated as a sensitive indicator of magma genesis and differentiation [1–4]. More recently, the precipitation of nanosized Fe-Ti-oxides during decompression has been associated to the intermittent explosive behavior of low-viscosity magmas [5]. Due to its strong tendency to segregate from the melt and crystallize, this oxide serves moreover as a widespread nucleating agent for the synthesis of glass-ceramics [6], while it represents a fundamental constituent of SiO_2-TiO_2 glasses/glass-ceramics that are appreciated for their low thermal expansion and catalytic activity [7–9].

The Ti^{4+} ion possesses an amphoteric or intermediate character with respect to those of the classically defined network formers and modifiers [10]. Its oxygen coordination in silicate melts exhibits a strong dependence on temperature, pressure and especially composition; it is generally pictured as a combination of coexisting tetrahedral, square-pyramidal and/or octahedral units [11–16]. Since low-coordinated species are predominant in silicate glasses [12,15], whereas Ti^{4+} is typically six-fold coordinated in the crystalline state [17], configurational changes are frequently associated with the precipitation of TiO_2-bearing crystals in a silicate melt [18,19]. Analogously, the glass forming ability of TiO_2-containing melts has been previously evaluated in terms of the ratio between low-coordinated species and modifier-like sixfold coordinated Ti^{4+}, such as in the SiO_2-TiO_2 compositional system [20].

This latter system, extensively studied in the past due to the above-mentioned technological importance, appears as a promising candidate for elucidating the solubility and structural role of Ti^{4+} in a simplified amorphous silicate matrix. Nevertheless, literature sources spanning over at least five decades provided occasionally contrasting views on the structural features of these glasses (a short review is proposed in Section 1.1). This is partially related to their high melting temperature and strong tendency to crystallize [21–23], which make the classical melt-quench route unfavorable, leading to a preference for other synthesis methods including flame hydrolysis and sol-gel processing.

This work was therefore conceived as a fundamental clarification of analogies and dissimilarities between SiO_2-TiO_2 glasses obtained by melt-quenching (or equivalently by flame hydrolysis, involving a very high sintering temperature) and by sol-gel processing. Combining Raman spectroscopy, solid-state nuclear magnetic resonance (NMR) and molecular dynamics (MD) simulations, we succeeded in developing an all-encompassing picture of the glass-forming region and structural features of these materials.

1.1 Review of relevant literature on SiO_2-TiO_2 amorphous materials

Studies based on conventional melting focused mostly on the determination of a phase diagram for the system (Fig. Sup1), involving a eutectic point at ~8 mol% TiO_2 and ~1550 °C [21] and a high-temperature liquid immiscibility field between ~20 mol% and ~90 mol% [23–25]. Despite the high melting temperatures and the strong devitrification tendency, some authors succeeded in characterizing SiO_2-TiO_2 glasses synthesized by electromelting, setting the limit of glass-forming ability at 10-12 mol% TiO_2 [26,27] and invariably assuming a tetrahedral or mixed tetrahedral-octahedral oxygen coordination for Ti^{4+} [26–29].

Nevertheless, large-scale production of monolithic glass samples has first been achieved by the flame hydrolysis method, in which a stoichiometric vapor mixture of suitable volatile precursors (such as $SiCl_4$ and $TiCl_4$) is oxidized in a CH_4-O_2 flame to obtain a fine glassy particulate that can be thereafter sintered at temperatures > 1700 °C [7]. The glass-forming region was macroscopically inferred to extend up to ~12.5 mol% [7]; early Raman and IR spectroscopic characterizations suggested again a tetrahedral or mixed tetrahedral-octahedral oxygen coordination of Ti^{4+} [30–32], in agreement with the reported solubility of TiO_2 in cristobalite up to ~8 mol% [33]. More direct investigations performed by X-ray absorption spectroscopy (XAS) at the Ti K-edge [34,35] revealed Ti^{4+} to be almost solely 4-fold coordinated in these glasses in the range 2-6 mol% TiO_2, with an increasing amount of octahedral species (still < 30% of the total) subsequently appearing up to 11.5 mol%, where the first crystalline TiO_2 polymorphs were detected. At impurity levels (TiO_2 < 0.03 mol%), Ti^{4+} would instead exhibit modifier-like 6-fold oxygen coordination. Later analyses by X-ray photoelectron spectroscopy [36], Raman and IR spectroscopy [37,38] and electron energy loss spectroscopy [39] did not substantially alter these views.

The sol-gel route, typically based on the condensation of sols containing hydrolyzed alkoxide precursors, started to be evaluated extensively in the 1980s as a possible alternative to the high melting temperatures of SiO_2-TiO_2 mixtures [40–42]; the potential use of these materials as porous substrates for catalytic applications particularly boosted scientific investigations [8]. Nevertheless, the choice of suitable synthesis parameters resulted crucial to avoid phase separation already in the sols or in the gels [43–45,45,46]. The need for drying the gels at relatively high temperatures to obtain fully interconnected glasses, moreover, appeared in clear conflict with the low thermal stability of these glasses [41,47,48]; notice that water could be still detected in SiO_2-TiO_2 amorphous materials after annealing at 900 °C [40] and a similar H_2O persistence was reported in gel-derived SiO_2 glass [49–52].

All these factors made the structural investigation of gel-derived SiO_2-TiO_2 glasses rather challenging. For instance, above ~6 mol% TiO_2, heterogeneity and TiO_2 crystallization affected the samples employed by Henderson and coworkers for their Raman and XAS studies [15,41,53–55]. Despite this, they inferred a mixed 4-fold and 5-fold coordination for Ti^{4+} in the glass, possibly involving the formation of oxygen triclusters; they associated 6-fold coordinated species to Ti-rich clusters. Concurrently, other

authors [56–63] adopted a multipronged approach including solid-state NMR, X-ray and neutron diffraction and XAS to elucidate the structural evolution of SiO_2-TiO_2 gels during condensation and annealing. According to their ultimate results, four possible environments are suggested for Ti^{4+} in these materials: 1) distorted octahedral oxygen coordination, prevalently in gels treated below 250 ºC and possibly corresponding to a tetrahedron with two further bonds to hydroxyl groups; more regular 2) tetrahedral and 3) octahedral units, dispersed in the amorphous structure of gel-derived glasses treated at relatively high temperature; 4) six-fold oxygen coordination in phase-separated TiO_2-rich clusters and crystals.

2. Experimental

2.1. Sol-gel glasses

Sol-gel glasses were produced as spray-dried nanobeads according to the method presented in a previous publication [9]. Two solutions were prepared, homogenized separately and mixed together in the desired ratios shortly before being spray-dried. The first solution contained tetraethoxysilane (TEOS, 99.0% (GC), Fluka), isopropanol, deionized water as a hydrolysis agent (molar ratio TEOS/H_2O = 0.25) and concentrated nitric acid (69%, Fluka) to adjust the pH to 1. The second solution was obtained by mixing equimolar amounts of Ti-butoxide (97.0%, Sigma-Aldrich) and ethyl acetoacetate (99.0%, Sigma-Aldrich) in isopropanol. Mixed solutions corresponding to samples with 5, 8, 10 and 17 mol% TiO_2 (respectively T5s, T8s, T10s and T17s in the following) were nebulized into a tube furnace set at 200 °C using an aerosol atomizer (Atomizer, AGK 2000, Palas) operated with pressurized air (2.8 bar); the resulting nanobeads (diameter between 50 and 200 nm) were collected from a particle filter at the other end of the furnace. Higher TiO_2 loadings (e.g. from 25 to 50 mol%) could be sprayed but proved unstable to the subsequent treatment at 600 °C (SI section, Fig. Sup2); they were therefore discarded from our further analyses. For the production of a glass containing 8 mol% TiO_2 and enriched in ^{17}O, the same procedure was applied, using ^{17}O-enriched water (enrichment degree: 40%, Cortecnet) for the hydrolysis of TEOS; the sample is noted as T8s(^{17}O).

2.2. Melt-quenched glasses

Melt-quenched glasses were prepared by aerodynamic levitation coupled to CO_2 laser heating (ADL), using a setup described in a previous work [64]. SiO_2 (Chempur, 99.9%) and TiO_2 (Evonik, Aeroxide TiO_2 P 25, 99.5%) powders were mixed thoroughly in an agate mortar and pressed into pellets of approximately 1 g. Small chunks of the pellets weighing from 10 to 50 mg were then melted using O_2 as a levitation gas, gradually increasing the laser power until reaching 1900-2100 °C (as recorded by two pyrometers). The levitated droplet was left at this temperature for a few seconds and then quenched by cutting the laser power; the cooling rate is estimated to be in the order of 300 K s^{-1} or more [64]. Using this

method, several glassy beads containing 0, 0.5, 1, 2, 4, 6, 8 and 10 mol% could be prepared; they were accordingly named T0m, T0.5m, T1m, T2m, T4m, T6m, T8m, T10m (-*m* for melt-quenched). In the range T0m-T6m, macroscopically homogeneous colorless beads could reproducibly be obtained, whereas TiO_2-richer compositions frequently exhibited opaque regions due to the crystallization of anatase, as confirmed by Raman spectroscopy. It was impossible to reliably obtain glassy samples with TiO_2 contents >10 mol%. All glassy beads were very rich in bubbles, due to the high viscosity of the materials at the employed melting temperatures, which also resulted in occasionally poor chemical homogenization of the melts (confirmed by SEM). Nevertheless, lower viscosities could not be attained due to physical limitations, since Si and Ti are increasingly volatile above 2000 °C [65]. An analytical strategy based on the analysis of a large number of samples was therefore adopted to overcome the uncertainties possibly arising from the occasional heterogeneity of the samples (see below).

In the attempt of synthesizing a melt-quenched glass enriched in ^{17}O, the as-sprayed sol-gel sample T8s(^{17}O) was placed in a tungsten crucible and melted at 1800 °C for 1 h in vacuum (to avoid exchanges with the atmospheric $^{16}O_2$), using a Setaram DTA/TGA SETSYS Evo 2400. The so-obtained material was partially crystallized; it is referred in the following as T8m(^{17}O).

2.3. Heat treatments

The as-prepared sol-gel materials required a further annealing stage to fully decompose the residues of their organic precursors, as also observed before [9]. A treatment at 450 °C for 12 h in air resulted insufficient: a strong photoluminescence still prevented the acquisition of Raman spectra with the selected laser line at 514 nm; heating at 600 °C for 12 h was found more suitable, although the glasses still contained substantial amounts of water. To dehydrate them, several drying protocols were then attempted in air using conventional laboratory furnaces, as detailed in Fig. 3-b: heating ramps were kept at 5 K s^{-1}, testing maximum temperatures between 900 °C and 1200 °C and isothermal segments from 1 h to 30 h.

In the case of sample T8s(^{17}O), the pre-emptive heat treatment at 600 °C was performed in Ar using a Setaram DTA/TGA SETSYS Evo 2400, to avoid exchanges with $^{16}O_2$ from the atmosphere; however, the sample still exhibited photoluminescence, so that the as-sprayed powder was subsequently treated also at 800 °C for 12 h, to enable its characterization by Raman spectroscopy. Different decomposition kinetics of the organic precursors according to the employed atmosphere have been previously reported [40].

TiO_2-bearing cristobalite was synthesized according to the procedure described by previous authors [33]: sample T5s was placed in a hot furnace at 1450 °C for 2 h and then quenched in air. For comparison, a TiO_2-free cristobalite sample was similarly produced, treating our SiO_2 raw material at 1600 °C for 4 h. These samples are respectively named as T5crist and T0crist in the following treatment.

2.4. Raman spectroscopy

Raman spectra were collected in parallel polarization using a Renishaw InVia Qontor spectrometer, mounting an Ar green laser (514 nm) and a holographic grating of 1800 lines/mm. The nominal laser power was generally set at 50 mW, but samples containing high amounts of TiO_2 and/or crystalline TiO_2 polymorphs required attenuation down to 1% of this power to avoid detector saturation. The measurements were performed with 15 s integration time and 6 accumulations, focusing 30-40 μm below the surface of the melt-quenched beads or on the gel-derived nanosized powders with a 50x objective. Numerous melt-quenched beads of each nominal composition were analyzed at several locations, to avoid partially crystallized regions and average out possible compositional inaccuracies deriving from occasionally poor homogenization of the melts. In the following data treatment (Fig. 2), at least three spectra for each melt-quenched composition were analyzed, after a first selection among several candidates.

Data evaluation involved a simple baseline subtraction between 80 and 1300 cm^{-1} (Figs. 3 and 4 examine a much wider spectral range and therefore report the raw spectra); the spectra were then normalized to their maximum intensity. To verify the appearance and growth of a Raman band at ~685 cm^{-1} (marked as T_1 in the following), the spectra shown in Figure 1 were smoothed and differentiated in the range 620-770 cm^{-1}; the slope of the first derivative was used to mathematically infer the concavity variation in this spectral region. Interpretation of the Raman spectra of crystalline materials was facilitated by the online consultation of the RRUFF database [66]: reference IDs are accordingly reported in the text.

2.5. X-ray diffraction (XRD)

The samples were characterized by XRD using a D8 Advance Bruker laboratory diffractometer (Bragg-Brentano geometry, Cu $K\alpha_{1,2}$ incident radiation, LynxEye XE line detector). The powders were placed on low-background flat Si sample holders and dispersed with a few ethanol droplets. Lattice parameters were computed by Le-Bail fits using the software HighScore Plus (Panalytical).

2.6. Transmission electron microscopy (TEM)

Sample T8m(^{17}O) was examined in a Philips CM20 TEM operated at 200 kV, performing bright- and dark-field imaging, selected area electron diffraction (SAED) and energy-dispersive X-ray spectroscopy (EDX) measurements. The powder was dispersed in ethanol, after which a droplet was deposited and dried on a copper grid layered by an amorphous holey carbon film.

2.7. Molecular dynamics simulation and DFT GIPAW computation

Classical molecular dynamics (MD) model structures of T10m glass were generated with rigid ion potentials using the DL_POLY 4 package, whose details are reported elsewhere [67,68]. This composition has been chosen to remain close to that of melt-quenched glasses while increasing the number of statistically relevant titanium atoms in the cell. Cubic boxes with 150 atoms were used and the edge lengths were adjusted to match the experimental density [7]. We used a previously proposed force field [69] in which interactions between Si-O, Ti-O and O-O are formalized by a Morse potential. Initial random structures were first equilibrated by a 100 ps NVT run at high temperature (3500 K), followed by quenching at a rate of 2.5 K ps^{-1} from 3500 K to 300 K. Six structures were created to increase the statistics.

For all obtained structural models, the atomic positions were optimized by DFT using the CASTEP package [70]. Computations of NMR chemical shielding and electric field gradient tensors were then performed using the Gauge Including Projector Augmented Waves (GIPAW) [71] and the Projector Augmented Waves (PAW) [72] methods respectively, as implemented in CASTEP. All computations were performed using the GGA PBE functional [73] and ultrasoft pseudopotentials (Materials Studio 7.0) generated "on-the-fly" [74]. Isotropic chemical shifts were calibrated based on series of computations performed on model crystalline systems of known structures, according to the relationships [75]:

$$\delta\left(^{29}Si\right) = -0.921\,\sigma\left(^{29}Si\right) + 289$$

$$\delta\left(^{17}O\right) = -0.946\,\sigma\left(^{17}O\right) + 252$$

where δ is the isotropic chemical shift and σ the corresponding chemical shielding.

NMR parameters were also computed for anatase and rutile TiO_2 models considering supercells of 384 and 576 atoms, respectively, and using the same setting as for MD structures. Structural and GIPAW calculations were analysed using a homemade python code. Atoms were clustered as a function of their speciation (i.e. coordination numbers, atom-linked…), calculating property distributions for each speciation. Distributions were smoothed by applying a Gaussian broadening to each point with broadness equal to the standard deviation of the dataset. The cut-off radius used to perform structural analyses was set to 2.2 Å for Si-O and Ti-O, corresponding to the first minimum of the partial distribution function. All structural analyses reported in the text below were performed on these DFT-optimized structures.

2.8. Solid-state nuclear magnetic resonance (NMR)

Only reproducibly amorphous samples were characterized by solid-state NMR, crushing and grinding several beads; the resulting powder was filled into ZrO_2 rotors. In addition, partially crystallized T8m(^{17}O) was also measured, to support the interpretation of ^{17}O Magic Angle Spinning (MAS) NMR spectra. ^{29}Si MAS NMR spectra were acquired on a Bruker Avance III spectrometer operating at a magnetic field of 7.0 T (^{29}Si Larmor frequency of ν_0=59.6 MHz) using a 4 mm probe. Spectra were recorded at a

spinning rate of 10 kHz using a 30° flip angle (radio frequency field of 55 kHz) and a recycle delay of 60 s to insure complete relaxation of the magnetization. Between 1000 and 3000 transients were collected for each spectrum. ^{29}Si chemical shifts are referenced relative to tetramethylsilane (TMS) at 0 ppm. Because the T8m(^{17}O) sample was only available in limited amount, a Carr-Purcell-Meiboom-Gill (CPMG) echo-train acquisition [76,77] was used to enhance the signal-to-noise ratio by summing 256 echoes equally spaced by a duration of 5.2 ms.

^{17}O MAS NMR spectra were acquired on a Bruker Avance III spectrometer operating at a magnetic field of 17.6 T (^{17}O Larmor frequency of ν_0=101.7 MHz) using a 2.5 mm probe. Quantitative spectra were recorded at a spinning rate of 33.33 kHz using a small flip angle of 10° (corresponding to a pulse duration of 0.55 µs). Between 16384 and 20480 transients were co-added with a recycle delay of 0.5 s. ^{17}O chemical shifts are referenced relative to water at 0 ppm. ^{17}O-{^{1}H} polarization transfer experiments allowing the selective observation of T-O-H moieties were performed using a refocused-INEPT [78,79] sequence with a SR421 recoupling block [80,81]. The RF field strengths for the $\pi/2$ and π pulses on the ^{17}O and ^{1}H channels were set to 20 and 78 kHz, respectively, while a ^{1}H RF field strength of 66.66 kHz corresponding to the $2\omega_R$ condition was used for the recoupling block. Recoupling delay was kept short (120 µs) in order to selectively probe short-range O-H distances.

^{29}Si FID were processed through a homemade python code using nmrglue and numpy libraries [82,83]. Gaussian apodization centered at the top of the signal was applied prior to Fourier transform with line broadening of 25 Hz for ^{29}Si and ^{17}O. Simulations of ^{17}O spectra were done with Dmfit software [84] and ^{29}Si ones were done using fNMR package [85].

3. Results

3.1 Glass-forming ability and overall examination

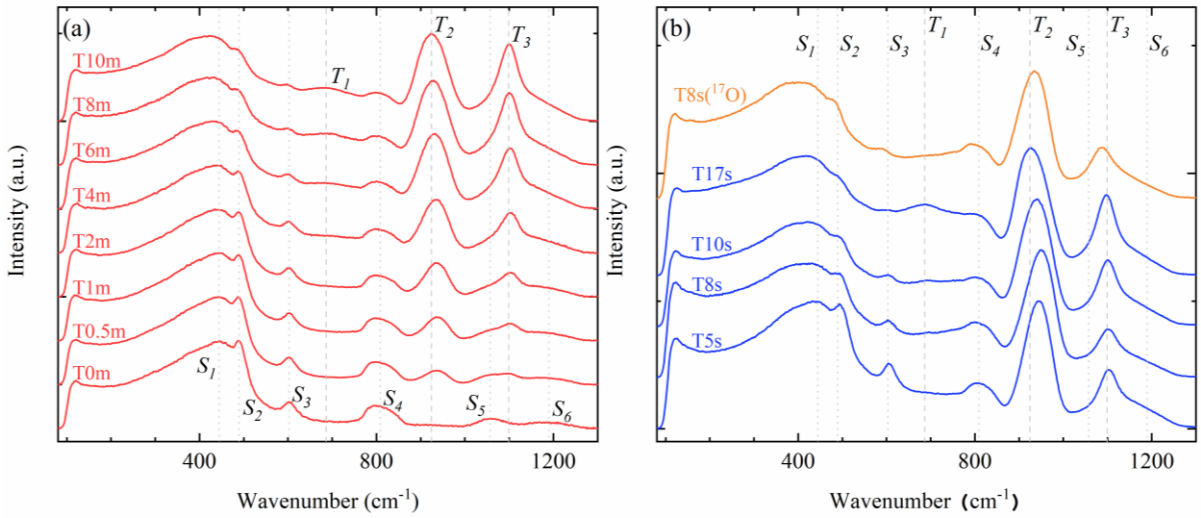

Figure 1. Raman spectra acquired from SiO_2-TiO_2 glasses obtained by different synthesis methods. a) Melt-quenched samples; b) gel-derived materials, treated at 600 °C for 12 h in air, excluding T8s(^{17}O) which was treated in Ar at 800 °C for 12 h. The main characteristic bands for vitreous SiO_2 are labelled as S_1, S_2, S_3, S_4, S_5 and S_6, while those related to the incorporation of Ti^{4+} are identified by T_1, T_2 and T_3; vertical lines are kept at the same position in both figures to facilitate the comparison.

The Raman spectra collected from melt-quenched materials (Fig 1-a) confirmed the formation of glasses and the successful incorporation of Ti^{4+} up to 10 mol% TiO_2. Sample T0m exhibited the typical vibrational features of vitreous SiO_2, labelled from S_1 to S_6. According to the available literature, S_1 and S_4 (the latter one possibly involving a LO-TO splitting) can be assigned to the vibrations of Si-O-Si linkages in the glass network [86–88]; S_2 and S_3 are also known as "defect lines", respectively stemming from the breathing modes of four- and three-membered rings of SiO_4 tetrahedra [89,90]; S_5 and S_6 were previously related to the asymmetric stretching of bridging oxygens linking SiO_4 tetrahedra, again with a LO-TO splitting [86–88] or possibly corresponding to two different sets of stretching vibrations [91]. Upon TiO_2 incorporation, the broad maximum S_1 shifted to lower wavenumbers, while S_2 and S_3 gradually subsided. In parallel, three supplementary Raman features became visible and increased in intensity, labelled as T_1, T_2 and T_3. The assignment of these bands is controversial in the available literature and will be addressed in higher detail in the Discussion section. Nevertheless, the position of the maximum of T_2 (Fig. 2-a), the concavity of the Raman spectra at T_1 (i.e. the slope of their 1st derivative, Fig. 2-b) and the intensity ratio T_2/T_3 (Fig. 2-c) exhibited an approximately linear correlation with the TiO_2 content of the melt-quenched glasses.

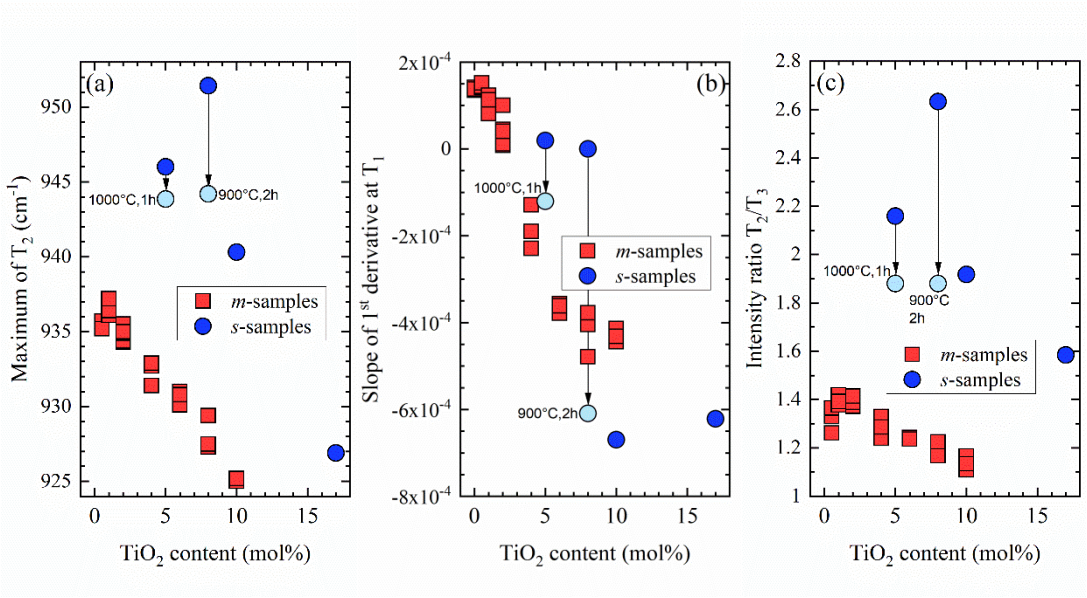

Figure 2. Representative indices computed from the Raman spectra of melt-quenched and gel-derived glasses (T8s(^{17}O) was disregarded due to the isotopic shift). a) Location of the maximum intensity for the Raman band labeled as T_2; b) slope of the 1st derivative of the Raman signal at the position of T_1; c) intensity ratio between T_2 and T_3. Light blue circles represent the values obtained for partially dehydrated (and still amorphous) gel-derived samples, namely T5s treated at 1000 °C for 1 h and T8s treated at 900 °C for 2 h (the spectra are reported in Fig. 3).

Gel-derived glasses treated at 600 °C for 12 hours in air (Fig 1-b) exhibited strong similarities with those of their melt-quenched counterparts; amorphous materials could be easily obtained up to 17 mol% TiO_2. However, the computation of the above-introduced indices (Fig. 2) highlighted a general shift of T_2 to higher wavenumbers, a lower visibility of T_1 and a much lower intensity of T_3 in comparison to melt-quenched glasses of similar composition; the defect bands S_2 and S_3 appeared moreover more pronounced (compare for instance T5s and T6m). As for sample T8s(^{17}O) (dried at 800 °C for 12 in Ar), its spectrum matched well with that of T8s but exhibited a slight overall shift to lower wavenumbers, in line with previous observations of the Raman spectrum of ^{18}O-subtituted SiO_2 [87]. The noticed differences between melt-quenched and gel-derived glasses were ascribed to the non-negligible water content of these latter, as demonstrated by Raman spectra collected over a wider range (Fig. 3). A broad band assignable to OH stretching vibrations was indeed clearly identifiable at ~3600 cm^{-1} [92,93], while it was absent in melt-quenched materials.

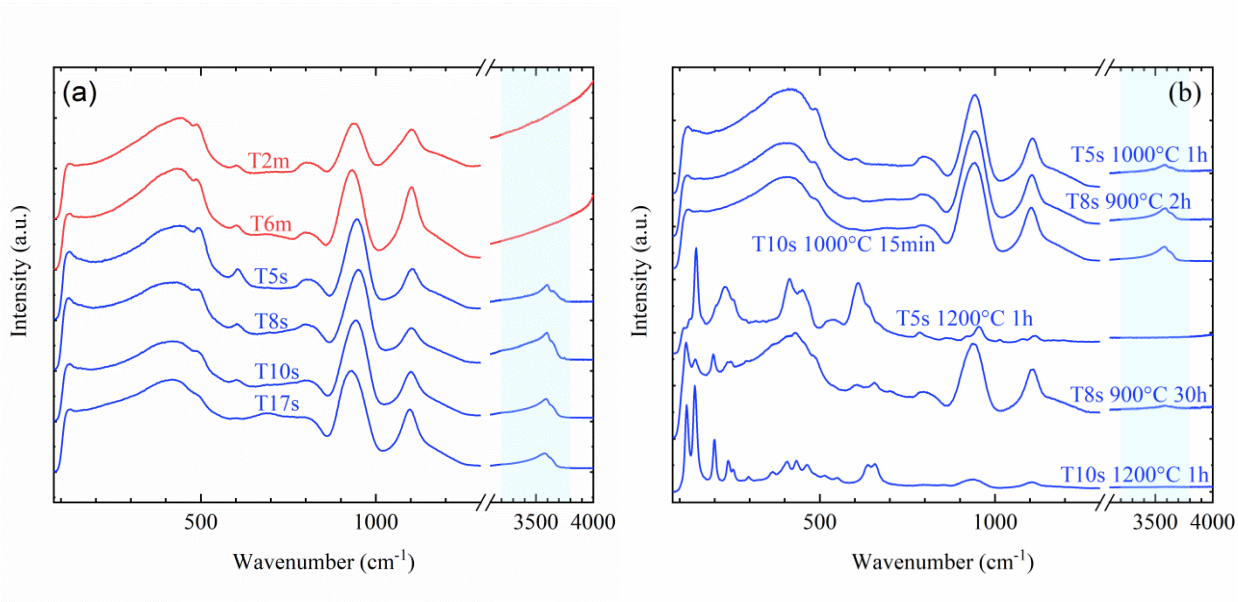

Figure 3. Raman spectra collected over a wider range (80 – 4200 cm^{-1}) from some of the samples. a) Melt-quenched glasses (as-prepared) and gel-derived glasses (pre-treated at 600 °C for 12 h), manifesting the presence of water in their structure; b) gel-derived glasses treated at various temperatures for up to 30 h, invariably exhibiting the onset of crystallization before full dehydration was completed.

Samples T5s, T8s and T10s were subjected to several tentative heat treatments at temperatures between 900 °C and 1200 °C: interestingly, partial dehydration of T5s (at 1000 °C for 1 h) and of T8s (at 900 °C for 2 h) led their spectra to resemble more closely those of their melt-quenched analogs, with a visible broadening of the defect bands S_2 and S_3 and an increase in the relative intensity of T_3, mirrored by a variation in the indices plotted on Fig. 2. However, full dehydration proved challenging to achieve before the onset of crystallization, marked by the appearance of sharper bands assignable to TiO_2(B), anatase [94], rutile and cristobalite (see references: [RRUFF-ID: R050031] and [RRUFF-ID: X050046]). As for T17s, previous investigations evidenced the emergence of TiO_2(B) and anatase crystals even only after 15 min at 800 °C [9]. Since treatments below the melting point were invariably affected by partial crystallization, full dehydration of gel-derived T8s(^{17}O) was attempted by complete melting at 1800 °C and subsequent quenching in vacuum (to avoid loss of ^{17}O to the atmosphere). The characterization by XRD and TEM of the resulting T8m(^{17}O) revealed that it was still for the most part amorphous (Fig. 4); however, the crystallization of few highly Ti-enriched noduli (composition qualitatively confirmed by EDX) could be detected, whose diffraction pattern was indexable as an oxygen-interstitial solid solution derived from metallic Ti [95], such as Ti_6O [ICDD 01-072-1471] or Ti_3O [ICDD 01-072-1806]. The Raman spectrum revealed the appearance at low wavenumbers of intense vibrational features characteristic for Ti-bearing crystals, which however did not completely obliterate the spectrum of the glass, hinting at a very low

crystalline volume fraction. Judging from its Raman spectrum, the residual glass was anhydrous and still contained some TiO_2 despite the partial crystallization, as confirmed by the clear persistence of the bands labeled as T_2 and T_3 and the absence of vibrational features at ~3600 cm^{-1}.

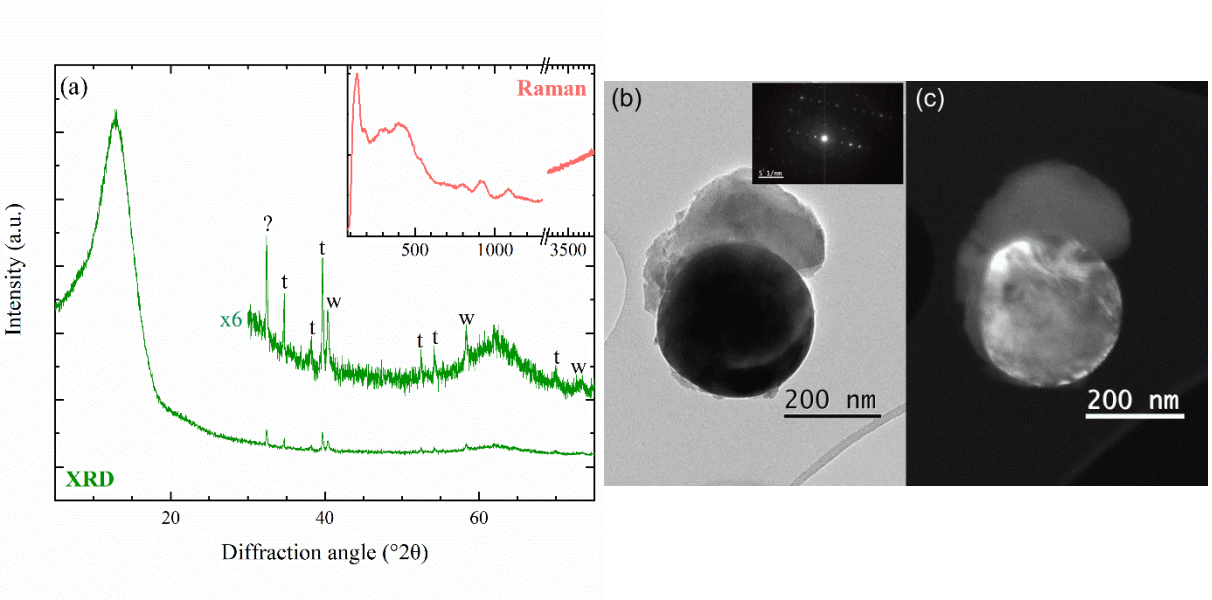

Figure 4. Experimental characterization of sample T8m(^{17}O), obtained by melting gel-derived T8s(^{17}O) at 1800 °C in vacuum. a) XRD pattern and Raman spectrum (inset) of the sample, manifesting the formation of small amounts of Ti-suboxide solid solutions (indexable as Ti_6O or Ti_3O) in an otherwise fully anhydrous and amorphous matrix (labels: *t* for Ti-suboxide solid solution, *w* for rests of the tungsten crucible). b) Bright-field and c) dark-field TEM micrographs of one of the Ti-enriched crystalline noduli found in the sample, with an inset exemplifying the well-defined electron diffraction patterns obtainable from them.

3.2 Structural characterization

3.2.1 Melt-quenched samples

Further investigations of the incorporation of Ti^{4+} in silica glasses were conducted using ^{17}O and ^{29}Si solid-state NMR, which have been shown to provide detailed information about chemical bonding and local structures in a variety of glasses [96–101]. For this purpose, a melt-quenched ^{17}O-enriched glass with nominal 8 mol% TiO_2 was synthesized as described above (Section 2.2).

As shown in Figure 5, the quantitative ^{17}O MAS NMR spectrum of sample T8m(^{17}O) exhibits two well-resolved ^{17}O central transition (CT) resonances and their associated satellite-transition (ST) spinning sideband manifolds, thereby revealing two distinct oxygen bonding environments in the glass structure. According to ^{17}O NMR literature data on SiO_2-TiO_2 materials [45,57,62], the intense line centered at 24.7 ppm and the broader one at 280 ppm can be assigned to bridging O_2Si and O_1Ti-1Si environments,

respectively. For the O_2Si moieties, the ^{17}O average isotropic chemical shift and quadrupolar coupling values (δ_{iso} = 41.3 ppm, C_Q = 5.33 MHz) obtained from the CT lineshape simulation assuming Gaussian distributions of δ_{iso} and C_Q are close to those reported for pure silica glass [102,103] (Tab. Sup1). Getting δ_{iso} and C_Q values for the O-1Ti-1Si resonance is more difficult because it shows a featureless central transition, in addition to satellite transition sidebands of low intensities. We only report the position of the CT barycenter ($\delta_{1/2}$) and notice that the <±3/2,±1/2> satellite transition sidebands are much broader than those of the O-2Si resonance suggesting a larger distribution of ^{17}O isotropic chemical shift for the O-1Ti-1Si moieties. Except for the ST spinning sidebands of O_2Si and O_1Ti-1Si, we note the absence of signals in the 400-800 ppm chemical shift range associated to oxygen atoms bonded to four, three or two titanium atoms [104]. The relative proportions of O_2Si and O_1Ti-1Si environments obtained from the fit of the spectrum (tacking into account all ST contributions) are 93% and 7%, respectively. This amount of Si-O-Ti bridging bonds is lower than expected (15 %) from the nominal composition, assuming a homogenous ^{17}O-enrichment of all T-O-T linkages in a fully polymerized random network of SiO_4 and TiO_4 tetrahedra. Since XRD and TEM revealed the formation of pseudo-metallic Ti-rich noduli in the sample, the observed lower proportion of O_1Ti-1Si contributions is likely due to a deviation from the starting composition of the glass, i.e. to a lower final TiO_2 content than the nominal. Nevertheless, this does not affect the overall interpretation of the ^{17}O MAS spectra.

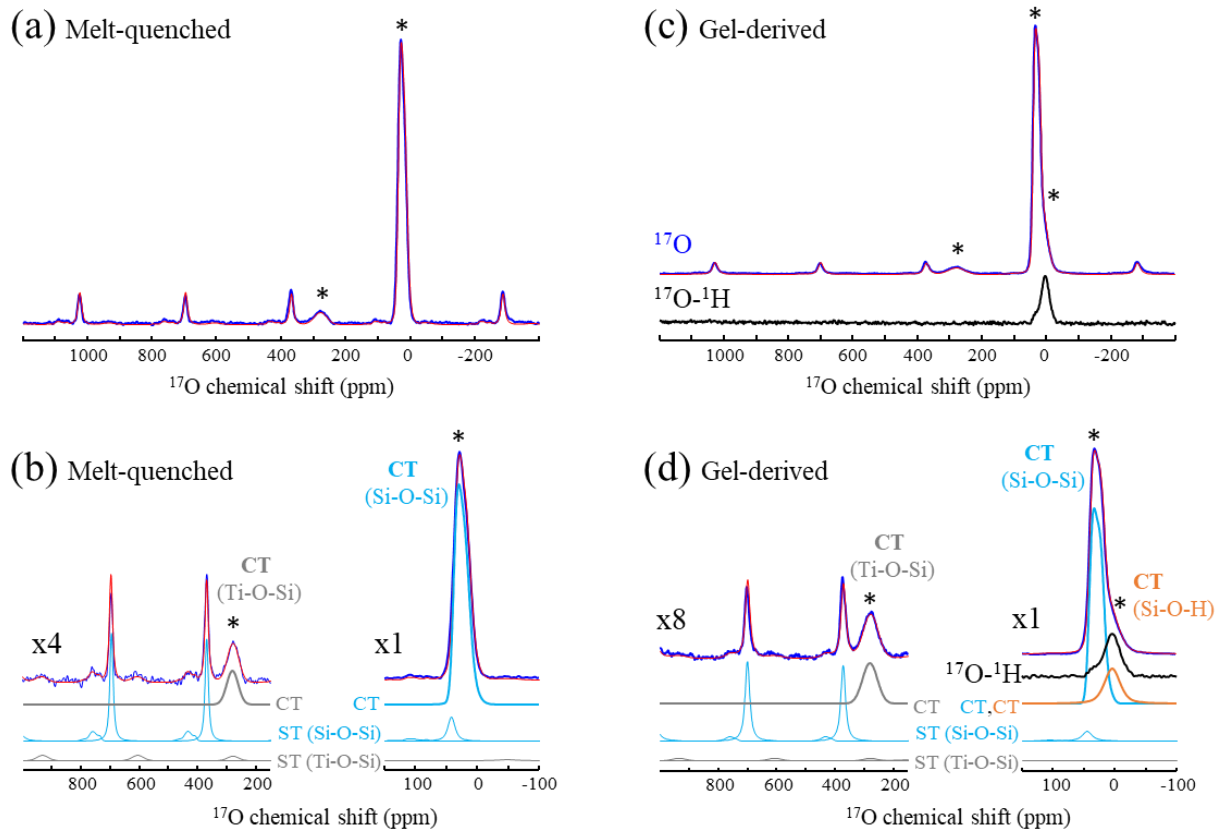

Figure 5. ^{17}O MAS NMR spectra of ^{17}O-enriched glasses: (a,b) melt-quenched T8m(^{17}O) and (c,d) gel-derived T8s(^{17}O), recorded at 17.6 T with a spinning rate of 33 kHz. The ^{17}O-^{1}H MAS spectrum of T8s(^{17}O) recorded using refocused-INEPT [78,79] polarization transfer with $SR4_2^1$ dipolar recoupling [80] is shown in black in (c,d). Expansions of the -100 to 150 and 150 to 1000 ppm frequency ranges are shown in (b,d). Experimental spectra and their simulations correspond to dark blue and red lines, respectively. CT lines and ST spinning sidebands patterns of O_2Si, O_1Si-1Ti and O_1Si-1H contributions are shown as light blue, grey and black lines, respectively.

To support the interpretation of the ^{17}O NMR results, DFT GIPAW computations of ^{17}O chemical shifts were performed for structural models with composition T10m. Six amorphous structures of 150 atoms were generated by classical force field molecular dynamics (MD) simulations and relaxed by DFT (at 0 K). Structural details of these models are given in Table Sup2 (see also .cif files and Fig. Sup4 in the supplementary materials). In all cases, MD simulations led to a fully polymerized tetrahedral network containing only SiO_4 and TiO_4 units, with no other higher-coordination polyhedral species (e.g. 5-fold or 6-fold coordinated Ti^{4+}, 5-fold coordinated Si^{4+}). The proportion of Si-O-Ti and Ti-O-Ti linkages exhibits a slight variability but, on average over the six structures, corresponds respectively to 18 and 1 % of the oxygen content, as expected from composition and assuming a random distribution of TiO_4 units in the

network. The average Ti-O bond length (1.83 Å) is found to be larger than the Si-O one (1.63 Å), in agreement with their ionic radii [105]; similarly, the average Si-O-Si bond angle (147.9°) is smaller than the Si-O-Ti one (150.1°). For the six amorphous structures, DFT GIPAW calculations lead to average ^{17}O isotropic chemical shift values of about 47 ppm for O_2Si and 312 ppm for O_1Si-1Ti environments (Figure 6, Table Sup3), in agreement with the proposed assignment. Moreover, the computations predict an average ^{17}O chemical shift difference of 265 ppm between oxygen atoms bridging two SiO_4 and those bridging one SiO_4 and one TiO_4 tetrahedral unit, with a larger distribution of ^{17}O isotropic chemical shift for the latter. These results closely mimic the observed frequency difference between the two ^{17}O signals (255.3 ppm), as well as the observed larger broadening of the O_1Si-1Ti <±3/2,±1/2> satellite transition sidebands, strongly supporting the formation of a fully polymerized silica-like network incorporating TiO_4 tetrahedral units up to several mol% TiO_2.

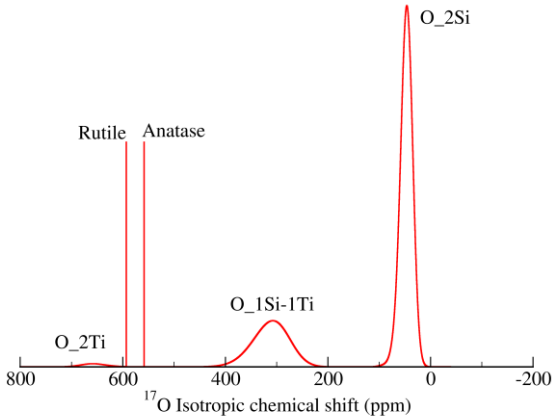

Figure 6. ^{17}O isotropic chemical shift distributions obtained from GIPAW calculations for the MD structural models with 10 mol% TiO_2. Average isotropic chemical shifts (and standard deviations) are 47.1 (8.7), 312.1 (25.1) and 656.1 (17.1) ppm for O_2Si, O_1Si_1Ti and O_2Ti environments in the MD models. Results of GIPAW calculations for O_3Ti environments in anatase and rutile TiO_2 are also provided for comparison.

The local structure of melt-quenched glasses up to 8 mol% TiO_2 was also investigated using ^{29}Si solid-state NMR. As depicted in Figure 7-a, the ^{29}Si MAS spectra of melt-quenched samples were very similar, almost independently of the titanium content. For the TiO_2-free silica glass, the ^{29}Si spectrum showed a broad resonance at – 110.0 ppm characteristic for Q^4 units and only a slight shift of 0.7 ppm toward lower frequency was observed upon TiO_2 additions up to 8 mol%. The weak variations in the ^{29}Si MAS spectra can be quantified by measuring the deviation from a Gaussian model lineshape which accounts for the spectrum acquired from the TiO_2-free silica glass (δ_{iso}= -110 ppm, fwhm=12.3), as

illustrated in Figure 7-b. Since ^{17}O NMR results indicate the formation of Si-O-Ti bonds, it shows that the ^{29}Si isotropic chemical shift is almost unchanged by the substitution of Si^{4+} by Ti^{4+} in the second coordination sphere of Q^4 units. This contrasts with the substitution of a silicon atom by a four-fold coordinated Al^{3+} or with the formation of a non-bridging oxygen atom, which lead to chemical shift variations of 5 and 10 ppm respectively [100]. The trend is confirmed by GIPAW computations of the MD amorphous models with 10 mol% of TiO_2, which allow to benchmark the ^{29}Si chemical shift ranges of Si-$(OSi)_4$ and Si-$(OSi)_3(OTi)$ moieties in a fully-polymerized network of SiO_4 and TiO_4 tetrahedra. Indeed, the ^{29}Si chemical shift ranges calculated for these two environments are found to overlap completely, with a difference of less than 0.7 ppm between their mean chemical shift values (Figure 7-c) and in good agreement with former computations of ^{29}Si chemical shifts in Ti-bearing zeolites (Ricchiardi and Sauer, 1999). In line with ^{17}O NMR results, the ^{29}Si MAS spectra thus suggest the formation of Si-O-Ti linkages with incorporation of titanium atoms as TiO_4 tetrahedral units in a fully polymerized network up to ~8-10 mol% TiO_2.

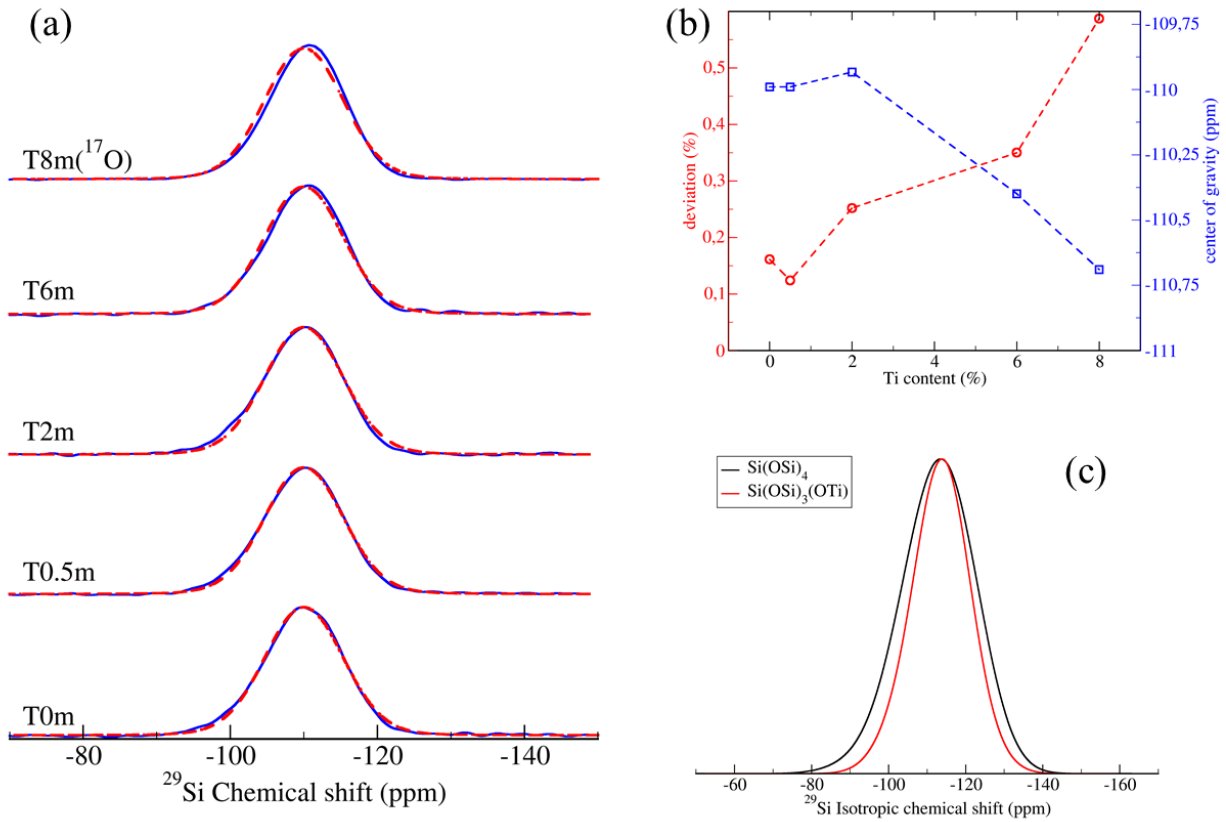

Figure 7. (a) ^{29}Si MAS NMR spectra of melt-quenched samples recorded at 7.0 T with a spinning rate of 10 kHz. Experimental spectra are shown in blue, while red dashed lines correspond to the best fit of the T0m spectrum with a Gaussian lineshape. (b) Percentage of difference between the experimental spectra

and the simulated spectrum of T0m (red circle, left axis) and position of the center of gravity of each spectrum (blue square, right axis). (c) ^{29}Si isotropic chemical shift distributions of $Si(OSi)_4$ and $Si(OSi)_3(OTi)$ environments obtained from GIPAW calculations for the MD models with 10 mol% TiO_2. Average isotropic chemical shifts (and standard deviations) are -112.7 (6.9) and -113.4 (5.6) ppm for $Si(OSi)_4$ and $Si(OSi)_3(OTi)$, respectively.

3.2.2 Sol-gel samples

As in the case of melt-quenched glasses, the nature of Ti^{4+} incorporation in gel-derived glasses was studied by ^{17}O NMR. The ^{17}O MAS spectrum of the gel-derived glass T8s(^{17}O) showed, in addition to the previously observed O_2Si and O_1Si-1Ti signals, a third contribution at lower chemical shift partially overlapping with the O_2Si CT peak (Figure 5). This new resonance located at 4.0 ppm could be selectively highlighted using ^{1}H-magnetization transfer experiments, revealing a short O-H distance and being therefore assigned to O_1Si-1H moieties in agreement with previous works [106,107]. A small variation of the ^{17}O isotropic chemical shift of bridging O_2Si (δ_{iso} = 43.1 ppm, C_Q = 5.19 MHz) is also observed with respect to the melt-quenched glass. The spectrum did not show any additional signal characteristic of Ti-O-Ti bonding, suggesting a homogeneous distribution of Ti atoms. Quantitative analysis of the spectrum gives relative proportions of 89, 7 and 4 % for bridging O_2Si, O_1Si-1Ti and non-bridging O_1Si-1H oxygen atoms, respectively. The proportion of O_1Si-1Ti is lower than expected from nominal composition, which could be associated to a preferential ^{17}O-enrichment of Si-O-Si linkages since TEOS was hydrolyzed separately with ^{17}O-enriched water during synthesis.

The ^{29}Si MAS NMR spectra of the gel-derived samples calcined at 600°C (Figure 8) showed obvious differences from those of melt-quenched glasses, with shoulders appearing at higher chemical shifts associated to depolymerized SiO_4 units. Indeed, ^{1}H-^{29}Si cross-polarization MAS spectra recorded at different contact times highlighted the presence of three distinct contributions located at -109.2, -100.5 and -91.5 ppm (see Figure Sup3). According to ^{29}Si chemical shift ranges, the peak at -109.2 ppm is assigned to both $Si(OSi)_4$ and $Si(OSi)_3(OTi)$ Q^4 units, while the line at -100.5 ppm is assigned to $Si(OSi)_3(OH)$ Q^3 units and the later one of much weaker intensity to $Si(OSi)_2(OH)_2$ Q^2 moieties. Simulations of quantitative spectra were done using the parameters extracted from CP MAS spectra and only the intensity of each component was varied. The position of the Q^4 line is found very similar with that observed for melt-quenched samples and the proportion of Q^2 moieties bearing two hydroxyl groups does not exceed 1% for all compositions heated at 600°C. A significant decrease of the relative proportion of Q^3 units is observed as the titanium content increases. For the T8s(^{17}O) sample, the amount of non-bridging oxygen atoms determined from the relative intensities of Q^n resonances is about 10 %. This corresponds to about twice the value obtained from the ^{17}O spectrum (4 %) suggesting a non-uniform ^{17}O-enrichment of the different

bonding environments in the T8s(^{17}O) sample. Apart from manifesting OH-bearing structural units, the ^{29}Si and ^{17}O spectra of gel-derived glasses show strong similarities with those of melt-quenched samples and remain consistent with the incorporation of four-fold coordinated Ti atoms in the silicate network at low TiO_2 content.

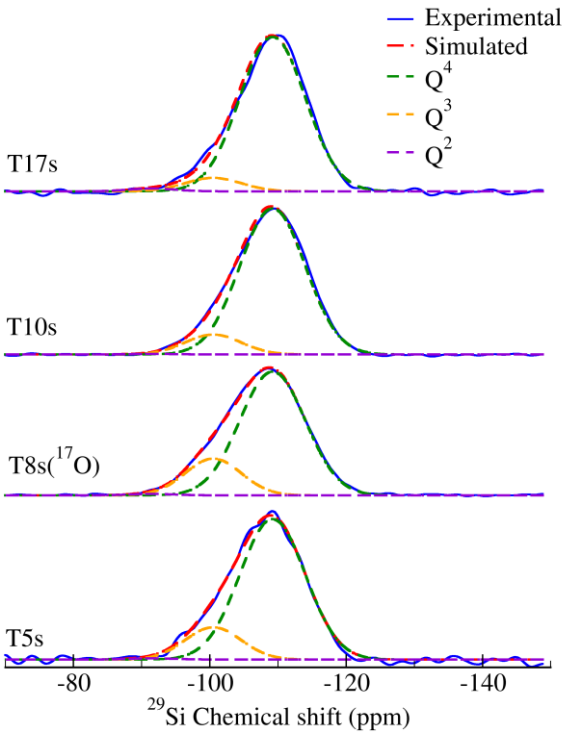

Figure 8. Experimental ^{29}Si NMR spectra of sol-gel samples (blue) and their simulations (dashed red). The individual Gaussian contributions associated to Q^4 ,Q^3 and Q^2 species are shown as dashed green, yellow and purple, respectively.

3.3 TiO_2-doped cristobalite

To support our discussion of SiO_2-TiO_2 glasses, we additionally synthesized TiO_2-doped cristobalite (sample T5crist) according to the devitrification method reported by previous authors [33]. The lattice parameters obtained from Le-Bail refinements of XRD data (Fig. 9) confirmed an expansion of the unit cell of cristobalite upon incorporation of Ti^{4+}, due to its larger effective ionic radius (0.42 Å) compared to Si^{4+} (0.26 Å) [105]; anatase and rutile were limited to trace levels in the sample. The Raman spectrum of T5crist resembled closely that of T0crist, excluding the bands assignable to an anatase impurity; nevertheless, two additional vibrational features could be discerned at high wavenumber, with maxima respectively at 955 cm^{-1} and 1115 cm^{-1}.

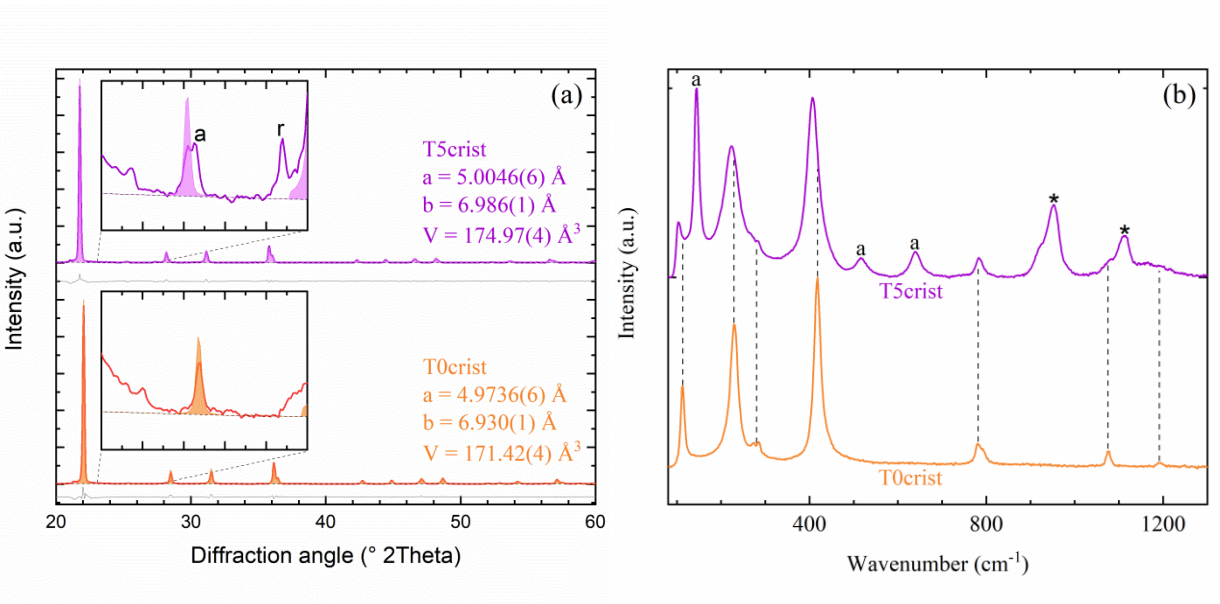

Figure 9. Results of the analytical characterization of samples T0crist and T5crist, devitrified respectively at 1600 °C and 1450 °C to form cristobalite. a) XRD patterns and related Le-Bail fits, detailing the lattice parameters obtained for cristobalite (filled areas: calculated intensity; broken line: background; gray line: fit residuals; *a* and *r* label the most intense peak of anatase and rutile, respectively); b) Raman spectra of the same samples (labels: *a* for anatase, * for Raman bands absent in the reference spectrum of tetragonal cristobalite [RRUFF-ID: X050046], to which all unmarked features can otherwise be related).

4. Discussion

The results of our study provide a self-consistent structural view on the formation of glasses in the binary system SiO_2-TiO_2. Anhydrous glasses can be obtained by melt-quenching at least up to 10 mol% TiO_2, despite the higher difficulty in quenching a homogeneously amorphous material as TiO_2 content increases. This observation is consistent with the available phase diagram [21,23], whose eutectic locates at ~8 mol%: beyond this point, the first phase predicted to form during cooling through the liquidus is rutile, whose ability to precipitate homogeneously in the volume can clearly affect glass-forming ability more than cristobalite, which is typically found at the surface. Moreover, the threshold of 10 mol% TiO_2 corresponds to the statistical emergence of Ti-O-Ti bonds in a random network of tetrahedral units (the most consistent structural description of SiO_2-TiO_2 glasses, see also below), as mirrored by the average values of our MD models in Tab. Sup2. In other words, the statistical presence of Ti-O-Ti direct linkages in the melt appears to be energetically unfavorable for glass formation (as supported by the energy differences between various relaxed MD models listed in Tab. Sup2), possibly representing the main structural driving force for the onset of crystal nucleation.

Concerning gel-derived glasses, we analyzed only materials up to 17 mol% TiO_2, since samples with 25 mol% and 50 mol% already exhibited crystalline features after the first calcination at 600 °C (SI, Fig. Sup2). Other authors reported the synthesis of gels of high TiO_2 content and similarly noted their high instability [40,41,44,48,56,57,59,108–110]. The predictable H_2O content of our samples, which can be roughly estimated as a few wt% based on our Raman [93] and ^{29}Si NMR spectra, persisted even after a pre-emptive drying stage at 600 °C, so that these materials should be consistently described as belonging to a ternary compositional system, i.e. SiO_2-TiO_2-H_2O. Obtaining dry glasses from these hydrous gels proved then rather challenging, probably also due to the lowering of viscosity and to the enhancement of nucleation usually noticed in water-bearing silicate melts [111–113]. Our observations therefore confirm the conclusions previously inferred from other compositional systems [114]: the sol-gel route does not seem to significantly enlarge the anhydrous glass-forming ability of reluctant glass-formers, due to the inevitable competition between dehydration and devitrification on the way to a fully densified glass. This scenario is in line with the updated definition of the glassy state of matter and its ultimate fate to crystallize [115], which disallow a spontaneous glass-to-crystal transformation. As for the observed formation of Ti-rich pseudo-metallic noduli in T8m(^{17}O) during melting at 1800 ºC in vacuum, it was clearly caused by the extreme reducing conditions, which were previously shown to even possibly lead to volatilization of silicon as gaseous SiO [116]. Notice that the non-detection of these pseudo-metallic noduli on the oxygen spectrum (expected in the O_2Ti range) can be explained by their low volume fraction, their minor oxygen content and also the short recycling delay used in the measurements, optimized for amorphous signals.

The computational prediction and experimental confirmation of the absence of an observable and quantifiable effect of Ti-O-Si bonding on the ^{29}Si NMR spectra of amorphous materials qualifies again the characterization of SiO_2-TiO_2 glasses as a challenging task. Yet, our data obtained from melt-quenched glasses corroborate full polymerization of the silicate network (only Q^4 species on the ^{29}Si spectra) upon actual incorporation of Ti in their structure; Si-O-Ti bonds are moreover clearly observable in the ^{17}O spectrum of T8m(^{17}O) (despite its partial crystallization). Relating these observations, Ti^{4+} must be isomorphously integrated into the silicate network, as previously proposed by various authors assuming a prevalent tetrahedral coordination for Ti^{4+} (at least at low TiO_2 content) in anhydrous and homogeneous SiO_2-TiO_2 glasses [27,28,34,35]. This conclusion is supported by the synthesis of Ti^{4+}-containing cristobalite, in which the transition metal necessarily substitutes Si^{4+} in the tetrahedral network sites. The Raman spectrum of this phase also exhibits two supplementary bands at 955 cm^{-1} and 1115 cm^{-1}, whose position is close to that of T_2 and T_3 in glasses, clearly supporting their assignment to the vibrational features of bridging oxygens related to a 4-coordinated network-forming Ti^{4+}; this assignment agrees with the majority of literature sources [27,29,30,32,117].

Regarding the Raman band T_1, its assignment is less straightforward: given its vicinity to the position of bands arising in most of the known TiO_2 polymorphs in the range 600-670 cm^{-1} [94,118,119], its interpretation as the signature for 6-coordinated Ti^{4+} species in the amorphous network is particularly tempting, as also claimed by previous authors [27]. This assignment would however imply the formation of 6-fold Ti^{4+} already at very low TiO_2 content (see the linear dependence from composition observed in Fig. 2-b), which is in clear antithesis with our MD simulations, NMR data and previous XAS investigations exhibiting no significant detection of 6-fold Ti^{4+} up to at least ~6 mol% TiO_2 [34,35]. Consequently, the Raman band may indeed originate from a 6-fold coordinated Ti^{4+} content at impurity level, made detectable due to the especially high Raman sensitivity of these species as compared to other techniques (the high scattering power of TiO_2 polymorphs is well known to Raman users); nevertheless, the vibrational feature could equally stem from an additional mode related to tetrahedrally coordinated Ti^{4+}, shifted from the typical positions observed in SiO_2 (e.g. the band S_4) or in GeO_2 [86].

Based on our data, we also do not find significant reasons for assigning Ti^{4+} to a 5-fold oxygen coordination, which was proposed to be the dominant configuration in gel-derived and partially crystallized SiO_2-TiO_2 glasses investigated by other authors [55]. Indeed, MD simulations produce structural models in which Ti^{4+} is invariably 4-fold coordinated. In addition, the presence of TiO_5 units is expected to lead to extra-coordinated (3-fold) oxygen atoms with higher chemical shift values, which can be excluded from the analyses of the ^{17}O NMR spectra. For the same reason, pronounced clustering of octahedrally coordinated Ti^{4+} in the amorphous state seems also unlikely, since no signal is detected around 600ppm on ^{17}O spectra. Moreover, pure TiO_2 has virtually no glass-forming ability and no other vibrational features are observed at lower wavenumber (100-300 cm^{-1}), where the most intense bands of TiO_2 crystals are typically found [94,118,119].

NMR data obtained from H_2O-bearing gel-derived glasses still revealed the presence of Q^3 species (^{29}Si spectra) and of Si-OH linkages (^{17}O spectra), demonstrating an incomplete dehydration/densification of their network even after a treatment at 600 °C for 12 h. The lower fraction of Q^3 species noticed in TiO_2-richer glasses could reflect the expected lower viscosity of these materials, allowing higher structural mobility and faster H_2O removal during the drying stages: a calorimetric effect interpretable as a glass transition was observed in T17s at ~675 °C [9], while the T_g of anhydrous T10m was previously estimated as ~1000 °C [7] and that of anhydrous SiO_2 as ~1200 °C [120]. More generally, water incorporation is likely to represent the crucial factor for the increased glass forming ability of hydrous SiO_2-TiO_2 glasses or, differently formulated, for the higher solubility of Ti^{4+} in gel-derived water-bearing silicate glasses: a partially depolymerized, less rigid network can probably more easily accommodate network distortions due to the substitution of Si^{4+} for the substantially larger Ti^{4+}, also avoiding energetically less favorable Ti-O-Ti direct linkages.

5. Conclusion

We used a combination of Raman spectroscopy, molecular dynamics, GIPAW computations and solid-state ^{29}Si and ^{17}O NMR as a powerful multipronged approach for the structural characterization of glasses. Taking into account all hypotheses proposed in the literature, we have been able to confirm that titanium prevalently assumes a tetrahedral oxygen coordination in anhydrous SiO_2-TiO_2 glasses and that the glass solubility of TiO_2 is limited to ~10 mol%. Gel-derived glasses can incorporate substantially higher amounts of TiO_2, most likely due to the depolymerizing effect of a non-negligible water content: this result suggests that dehydration may be crucial in driving the crystallization of transition metal oxides in melts. All in all, the sol-gel route does not appear a viable solution for enlarging the glass-forming range of anhydrous silicates.

Acknowledgements

A.Z. wishes to acknowledge the Deutsche Forschungsgemeinschaft (DFG) for funding his research through the Walter Benjamin Program, grant no. ZA 1188/1-1. Also J.D. and G.H. acknowledge the support of DFG, grant no. DE 598/33-1. The authors are additionally grateful to: (i) Vinzent Olszok and Prof. Alfred P. Weber, for the assistance during the synthesis of spray-dried nanobeads at the Institute of Particle Technology at TU Clausthal; (ii) the ICMN laboratory (Orléans, France) for TEM access and Dr. Cécile Genevois as an operator; (iii) the French Agency for Research for its financial support through the Equipex Planex ANR-11-EQPX-36; (iv) the TGIR-RMN-THC Fr3050 CNRS for its financial support and (v) the CaSciModOT project (Calcul Scientifique et la Modélisation à Orléans et Tours) for the access to high performance computing facilities.

References

[1] F.J. Ryerson, E.B. Watson, Rutile saturation in magmas: implications for TiNbTa depletion in island-arc basalts, Earth and Planetary Science Letters. 86 (1987) 225–239. https://doi.org/10.1016/0012-821X(87)90223-8.

[2] G.A. Gaetani, P.D. Asimow, E.M. Stolper, A model for rutile saturation in silicate melts with applications to eclogite partial melting in subduction zones and mantle plumes, Earth and Planetary Science Letters. 272 (2008) 720–729. https://doi.org/10.1016/j.epsl.2008.06.002.

[3] K. Kularatne, A. Audétat, Rutile solubility in hydrous rhyolite melts at 750–900°C and 2kbar, with application to titanium-in-quartz (TitaniQ) thermobarometry, Geochimica et Cosmochimica Acta. 125 (2014) 196–209. https://doi.org/10.1016/j.gca.2013.10.020.

[4] F.P. Leitzke, R.O.C. Fonseca, J. Göttlicher, R. Steininger, S. Jahn, C. Prescher, M. Lagos, Ti K-edge XANES study on the coordination number and oxidation state of Titanium in pyroxene, olivine, armalcolite, ilmenite, and silicate glass during mare basalt petrogenesis, Contrib Mineral Petrol. 173 (2018) 103. https://doi.org/10.1007/s00410-018-1533-7.

[5] D. Di Genova, R.A. Brooker, H.M. Mader, J.W.E. Drewitt, A. Longo, J. Deubener, D.R. Neuville, S. Fanara, O. Shebanova, S. Anzellini, F. Arzilli, E.C. Bamber, L. Hennet, G. La Spina, N. Miyajima, In situ observation of nanolite growth in volcanic melt: A driving force for explosive eruptions, Science Advances. 6 (2020). https://doi.org/10.1126/sciadv.abb0413.

[6] W. Höland, G.H. Beall, Principles of Designing Glass-Ceramic Formation, in: Glass-Ceramic Technology, John Wiley & Sons, Ltd, 2019: pp. 1–66. https://doi.org/10.1002/9781119423737.ch1.

[7] P.C. Schultz, Binary Titania-Silica Glasses Containing 10 to 20 Wt% TiO2, Journal of the American Ceramic Society. 59 (1976) 214–219. https://doi.org/10.1111/j.1151-2916.1976.tb10936.x.

[8] A. Baiker, P. Dollenmeier, M. Glinski, A. Reller, Selective catalytic reduction of nitric oxide with ammonia: II. Monolayers of Vanadia Immobilized on Titania—Silica Mixed Gels, Applied Catalysis. 35 (1987) 365–380. https://doi.org/10.1016/S0166-9834(00)82873-0.

[9] A. Zandona, A. Martínez Arias, M. Gutbrod, G. Helsch, A.P. Weber, J. Deubener, Spray-Dried TiO2(B)-Containing Photocatalytic Glass-Ceramic Nanobeads, Adv. Funct. Mater. (2020) 2007760. https://doi.org/10.1002/adfm.202007760.

[10] A. Dietzel, Die Kationenfeldstärken und ihre Beziehungen zu Entglasungsvorgängen, zur Verbindungsbildung und zu den Schmelzpunkten von Silicaten, Zeitschrift Für Elektrochemie Und Angewandte Physikalische Chemie. 48 (1942) 9–23. https://doi.org/10.1002/bbpc.19420480104.

[11] D.B. Dingwell, E. Paris, F. Seifert, A. Mottana, C. Romano, X-ray absorption study of Ti-bearing silicate glasses, Phys Chem Minerals. 21 (1994). https://doi.org/10.1007/BF00203924.

[12] F. Farges, G.E. Brown, A. Navrotsky, H. Gan, J.J. Rehr, Coordination chemistry of Ti(IV) in silicate glasses and melts: II. Glasses at ambient temperature and pressure, Geochimica et Cosmochimica Acta. 60 (1996) 3039–3053. https://doi.org/10.1016/0016-7037(96)00145-7.

[13] F. Farges, G.E. Brown, A. Navrotsky, H. Gan, J.R. Rehr, Coordination chemistry of Ti(IV) in silicate glasses and melts: III. Glasses and melts from ambient to high temperatures, Geochimica et Cosmochimica Acta. 60 (1996) 3055–3065. https://doi.org/10.1016/0016-7037(96)00146-9.

[14] C. Romano, E. Paris, B.T. Poe, G. Giuli, D.B. Dingwell, A. Mottana, Effect of aluminum on Ti-coordination in silicate glasses: A XANES study, American Mineralogist. 85 (2000) 108–117. https://doi.org/10.2138/am-2000-0112.

[15] G.S. Henderson, X. Liu, M.E. Fleet, A Ti L-edge X-ray absorption study of Ti-silicate glasses, Physics and Chemistry of Minerals. 29 (2002) 32–42. https://doi.org/10.1007/s002690100208.

[16] E.T. Nienhuis, J. Marcial, T. Robine, C. Le Losq, D.R. Neuville, M.C. Stennett, N.C. Hyatt, J.S. McCloy, Effect of Ti4+ on the structure of nepheline (NaAlSiO4) glass, Geochimica et Cosmochimica Acta. 290 (2020) 333–351. https://doi.org/10.1016/j.gca.2020.09.015.

[17] F. Farges, G.E. Brown, J.J. Rehr, Coordination chemistry of Ti(IV) in silicate glasses and melts: I. XAFS study of titanium coordination in oxide model compounds, Geochimica et Cosmochimica Acta. 60 (1996) 3023–3038. https://doi.org/10.1016/0016-7037(96)00144-5.

[18] F. Farges, G.E. Brown, Coordination chemistry of titanium (IV) in silicate glasses and melts: IV. XANES studies of synthetic and natural volcanic glasses and tektites at ambient temperature and pressure, Geochimica et Cosmochimica Acta. 61 (1997) 1863–1870. https://doi.org/10.1016/S0016-7037(97)00050-1.
[19] L. Cormier, O. Dargaud, N. Menguy, G.S. Henderson, M. Guignard, N. Trcera, B. Watts, Investigation of the Role of Nucleating Agents in MgO−SiO2−Al2O3−SiO2−TiO2 Glasses and Glass-Ceramics: A XANES Study at the Ti K- and L2,3-Edges, Crystal Growth & Design. 11 (2011) 311–319. https://doi.org/10.1021/cg101318p.
[20] D.L. Evans, Glass structure: The bridge between the molten and crystalline states, Journal of Non-Crystalline Solids. 52 (1982) 115–128. https://doi.org/10.1016/0022-3093(82)90285-X.
[21] E.N. Bunting, Phase equilibria in the systems TiO2, TiO2-SiO2 and TiO2-Al2O3, BUR. STAN. J. RES. 11 (1933) 719. https://doi.org/10.6028/jres.011.049.
[22] R.W. Ricker, F.A. Hummel, Reactions in the System TiO2-SiO2; Revision of the Phase Diagram, J American Ceramic Society. 34 (1951) 271–279. https://doi.org/10.1111/j.1151-2916.1951.tb09129.x.
[23] R.C. DeVries, R. Roy, E.F. Osborn, Phase Equilibria in the System CaO-TiO2–SiO2, Journal of The American Ceramic Society. 38 (1955) 158–171.
[24] S.A. Kirillova, V.I. Almjashev, V.V. Gusarov, Phase Relationships in the SiO2–TiO2 System, 56 (2011) 9.
[25] C. Zhang, X. Ge, Q. Hu, F. Yang, P. Lai, C. Shi, W. Lu, J. Li, Atomic scale structural analysis of liquid immiscibility in binary silicate melt: A case of SiO2–TiO2 system, Journal of Materials Science & Technology. 53 (2020) 53–60.
[26] D.G. Ostrizhko, G.A. Pavlova, Structure of Glasses in the Silicon Dioxide Titanium Dioxide System, Izv. Akad. Nauk SSR, Neorg. Mat. 6 (1970) 74–77.
[27] B.G. Varshal, V.N. Denisov, B.N. Mavrin, G.A. Parlova, V.B. Podobedov, Kh.E. Sterin, Spectra of Raman and hyper-Raman light scattering of the TiO2-SiO2 glass system, Opt. Spektrosk. 47 (1979) 619–622.
[28] P.P. Bihuniak, R.A. Condrate, Structures, spectra and related properties of group IVB-doped vitreous silica, Journal of Non-Crystalline Solids. 44 (1981) 331–343. https://doi.org/10.1016/0022-3093(81)90036-3.
[29] K. Kusabiraki, Infrared and raman spectra of vitreous silica and sodium silicates containing titanium, Journal of Non-Crystalline Solids. 95–96 (1987) 411–417. https://doi.org/10.1016/S0022-3093(87)80138-2.
[30] M.C. Tobin, T. Baak, Raman Spectra of Some Low-Expansion Glasses, J. Opt. Soc. Am. 58 (1968) 1459. https://doi.org/10.1364/JOSA.58.001459.
[31] C.F. Smith, R.A. Condrate, W.E. Votava, The Difference Infrared Spectra of Titanium-Containing Vitreous Silica, Appl Spectrosc. 29 (1975) 79–81. https://doi.org/10.1366/000370275774455437.
[32] H.R. Chandrasekhar, M. Chandrasekhar, M.H. Manghnani, Phonons in TiO2–SiO2 glasses, Journal of Non-Crystalline Solids. 40 (1980) 567–575. https://doi.org/10.1016/0022-3093(80)90130-1.
[33] D.L. Evans, Solid Solution of TiO2 in SiO2, Journal of the American Ceramic Society. 53 (1970) 418–418. https://doi.org/10.1111/j.1151-2916.1970.tb12146.x.
[34] D.R. Sandstrom, F.W. Lytle, P.S.P. Wei, R.B. Greegor, J. Wong, P. Schultz, Coordination of Ti in TiO2 SiO2 glass by X-ray absorption spectroscopy, Journal of Non-Crystalline Solids. 41 (1980) 201–207. https://doi.org/10.1016/0022-3093(80)90165-9.
[35] R.B. Greegor, F.W. Lytle, D.R. Sandstrom, J. Wong, P. Schultz, Investigation of TiO2-SiO2 Glasses by X-ray absorption spectroscopy, Journal of Non-Crystalline Solids. 55 (1983) 27–43.
[36] S.M. Mukhopadhayay, S.H. Garofalini, Surface studies of TiO2–SiO2 glasses by X-ray photoelectron spectroscopy, Journal of Non-Crystalline Solids. 126 (1990) 202–208. https://doi.org/10.1016/0022-3093(90)90820-C.

[37] A. Chmel, G.M. Eranosyan, A.A. Kharshak, Vibrational spectroscopic study of Ti-substituted SiO2, Journal of Non-Crystalline Solids. 146 (1992) 213–217. https://doi.org/10.1016/S0022-3093(05)80493-4.
[38] S. Richter, D. Möncke, F. Zimmermann, E.I. Kamitsos, L. Wondraczek, A. Tünnermann, S. Nolte, Ultrashort pulse induced modifications in ULE - from nanograting formation to laser darkening, Opt. Mater. Express. 5 (2015) 1834–1850. https://doi.org/10.1364/OME.5.001834.
[39] S.C. Cheng, Coordination and optical attenuation of TiO2–SiO2 glass by electron energy loss spectroscopy, Journal of Non-Crystalline Solids. 354 (2008) 3735–3741. https://doi.org/10.1016/j.jnoncrysol.2008.03.045.
[40] C.J.R. Gonzalez-Oliver, P.F. James, H. Rawson, Silica and silica-titania glasses prepared by the sol-gel process, Journal of Non-Crystalline Solids. 48 (1982) 129–152. https://doi.org/10.1016/0022-3093(82)90251-4.
[41] T. Hayashi, T. Yamada, H. Saito, Preparation of titania-silica glasses by the gel method, J Mater Sci. 18 (1983) 3137–3142. https://doi.org/10.1007/BF00700798.
[42] M. Emili, L. Incoccia, S. Mobilio, G. Fagherazzi, M. Guglielmi, Structural investigations of TiO2-SiO2 glassy and glass-ceramic materials prepared by the sol-gel method, Journal of Non-Crystalline Solids. 74 (1985) 129–146. https://doi.org/10.1016/0022-3093(85)90407-7.
[43] M. Schraml-Marth, K.L. Walther, A. Wokaun, B.E. Handy, A. Baiker, Porous silica gels and TiO2/SiO2 mixed oxides prepared via the sol-gel process: characterization by spectroscopic techniques, Journal of Non-Crystalline Solids. 143 (1992) 93–111. https://doi.org/10.1016/S0022-3093(05)80557-5.
[44] M. Beghi, P. Chiurlo, L. Costa, M. Palladino, M.F. Pirini, Structural investigation of the silica-titania gel/glass transition, Journal of Non-Crystalline Solids. 145 (1992) 175–179. https://doi.org/10.1016/S0022-3093(05)80451-X.
[45] L. Delattre, F. Babonneau, 17O Solution NMR Characterization of the Preparation of Sol−Gel Derived SiO2/TiO2 and SiO2/ZrO2 Glasses, Chem. Mater. 9 (1997) 2385–2394. https://doi.org/10.1021/cm970372f.
[46] C. Gervais, F. Babonneau, M.E. Smith, Detection, Quantification, and Magnetic Field Dependence of Solid-State 17O NMR of X−O−Y (X,Y = Si,Ti) Linkages: Implications for Characterizing Amorphous Titania-Silica−Based Materials, J. Phys. Chem. B. 105 (2001) 1971–1977. https://doi.org/10.1021/jp003519q.
[47] D.S. Knight, C.G. Pantano, W.B. White, Raman spectra of gel-prepared titania-silica glasses, Materials Letters. 8 (1989) 156–160. https://doi.org/10.1016/0167-577X(89)90182-1.
[48] I.M.M. Salvado, J.M.F. Navarro, Phase separation in materials of the systems TiO2-SiO2 and ZrO2-SiO2 prepared by the alkoxide route, Journal of Materials Science Letters. 9 (1990) 173–176. https://doi.org/10.1007/BF00727707.
[49] R. Puyané, P.F. James, H. Rawson, Preparation of silica and soda-silica glasses by the sol-gel process, Journal of Non-Crystalline Solids. 41 (1980) 105–115. https://doi.org/10.1016/0022-3093(80)90196-9.
[50] A. Bertoluzza, C. Fagnano, M. Antonietta Morelli, V. Gottardi, M. Guglielmi, Raman and infrared spectra on silica gel evolving toward glass, Journal of Non-Crystalline Solids. 48 (1982) 117–128. https://doi.org/10.1016/0022-3093(82)90250-2.
[51] L.C. Klein, T.A. Gallo, G.J. Garvey, Densification of monolithic silica gels below 1000°C, Journal of Non-Crystalline Solids. 63 (1984) 23–33. https://doi.org/10.1016/0022-3093(84)90383-1.
[52] T.A. Gallo, L.C. Klein, Apparent viscosity of sol-gel processed silica, Journal of Non-Crystalline Solids. 82 (1986) 198–204. https://doi.org/10.1016/0022-3093(86)90131-6.
[53] G.S. Henderson, M.E. Fleet, The structure of Ti silicate glasses by micro-Raman spectroscopy, The Canadian Mineralogist. 33 (1995) 399–408.
[54] G.S. Henderson, M.E. Fleet, The structure of titanium silicate glasses investigated by Si K-edge X-ray absorption spectroscopy, Journal of Non-Crystalline Solids. 211 (1997) 214–221. https://doi.org/10.1016/S0022-3093(96)00640-0.

[55] G.S. Henderson, X. Liu, M.E. Fleet, Titanium coordination in silicate glasses investigated using O K-edge X-ray absorption spectroscopy, Mineralogical Magazine. 67 (2003) 597–607. https://doi.org/10.1180/0026461036740120.
[56] M.E. Smith, H.J. Whitfield, Application of oxygen-17 NMR spectroscopy to detection of atomic scale phase separation in titania-silica gels, J. Chem. Soc., Chem. Commun. (1994) 723. https://doi.org/10.1039/c39940000723.
[57] P.J. Dirken, M.E. Smith, H.J. Whitfield, 17O and 29Si Solid State NMR Study of Atomic Scale Structure in Sol-Gel-Prepared TiO2-SiO2 Materials, J. Phys. Chem. 99 (1995) 395–401. https://doi.org/10.1021/j100001a059.
[58] J.S. Rigden, J.K. Walters, P.J. Dirken, M.E. Smith, G. Bushnell-Wye, W.S. Howells, R.J. Newport, The role of titanium in : mixed sol-gels: an x-ray and neutron diffraction study, J. Phys.: Condens. Matter. 9 (1997) 4001–4016. https://doi.org/10.1088/0953-8984/9/20/001.
[59] R. Anderson, G. Mountjoy, M.E. Smith, R.J. Newport, An EXAFS study of silica–titania sol–gels, Journal of Non-Crystalline Solids. 232–234 (1998) 72–79. https://doi.org/10.1016/S0022-3093(98)00373-1.
[60] G. Mountjoy, D.M. Pickup, G.W. Wallidge, R. Anderson, J.M. Cole, R.J. Newport, M.E. Smith, XANES Study of Ti Coordination in Heat-Treated (TiO2)x(SiO2)1-x Xerogels, Chem. Mater. 11 (1999) 1253–1258. https://doi.org/10.1021/cm980644u.
[61] G. Mountjoy, D.M. Pickup, G.W. Wallidge, J.M. Cole, R.J. Newport, M.E. Smith, In-situ high-temperature XANES observations of rapid and reversible changes in Ti coordination in titania–silica xerogels, Chemical Physics Letters. 304 (1999) 150–154. https://doi.org/10.1016/S0009-2614(99)00302-4.
[62] D.M. Pickup, F.E. Sowrey, R.J. Newport, P.N. Gunawidjaja, K.O. Drake, M.E. Smith, The Structure of TiO2−SiO2 Sol−Gel Glasses from Neutron Diffraction with Isotopic Substitution of Titanium and 17O and 49Ti Solid-State NMR with Isotopic Enrichment, J. Phys. Chem. B. 108 (2004) 10872–10880. https://doi.org/10.1021/jp049053j.
[63] G.W. Wallidge, R. Anderson, G. Mountjoy, D.M. Pickup, P. Gunawidjaja, R.J. Newport, M.E. Smith, Advanced physical characterisation of the structural evolution of amorphous (TiO2)x(SiO2)1−xsol-gel materials, Journal of Materials Science. 39 (2004) 6743–6755. https://doi.org/10.1023/B:JMSC.0000045604.02983.96.
[64] A. Zandonà, M. Moustrous, C. Genevois, E. Véron, A. Canizarès, M. Allix, Glass-forming ability and ZrO2 saturation limits in the magnesium aluminosilicate system, Ceramics International. (2021). https://doi.org/10.1016/j.ceramint.2021.12.051.
[65] Leo. Brewer, Thermodynamic Properties of the Oxides and their Vaporization Processes., Chem. Rev. 52 (1953) 1–75. https://doi.org/10.1021/cr60161a001.
[66] B. Lafuente, R.T. Downs, H. Yang, N. Stone, 1. The power of databases: The RRUFF project, in: Highlights in Mineralogical Crystallography, De Gruyter, Berlin, Boston, 2015: pp. 1–30. https://doi.org/10.1515/9783110417104-003.
[67] I.T. Todorov, W. Smith, K. Trachenko, M.T. Dove, DL_POLY_3: new dimensions in molecular dynamics simulations via massive parallelism, J. Mater. Chem. 16 (2006) 1911–1918. https://doi.org/10.1039/B517931A.
[68] K. Okhotnikov, B. Stevensson, M. Edén, New interatomic potential parameters for molecular dynamics simulations of rare-earth (RE = La, Y, Lu, Sc) aluminosilicate glass structures: exploration of RE3+ field-strength effects, Phys. Chem. Chem. Phys. 15 (2013) 15041–15055. https://doi.org/10.1039/C3CP51726H.
[69] G. Malavasi, A. Pedone, M.C. Menziani, Towards a quantitative rationalization of multicomponent glass properties by means of molecular dynamics simulations, Null. 32 (2006) 1045–1055. https://doi.org/10.1080/08927020600932793.
[70] S.J. Clark, M.D. Segall, C.J. Pickard, P.J. Hasnip, M.I.J. Probert, K. Refson, M.C. Payne, First principles methods using CASTEP, Zeitschrift Für Kristallographie - Crystalline Materials. 220 (2005) 567–570. https://doi.org/doi:10.1524/zkri.220.5.567.65075.

[71] C.J. Pickard, F. Mauri, All-electron magnetic response with pseudopotentials: NMR chemical shifts, Phys. Rev. B. 63 (2001) 245101. https://doi.org/10.1103/PhysRevB.63.245101.
[72] M. Profeta, F. Mauri, C.J. Pickard, Accurate First Principles Prediction of 17O NMR Parameters in SiO2: Assignment of the Zeolite Ferrierite Spectrum, J. Am. Chem. Soc. 125 (2003) 541–548. https://doi.org/10.1021/ja027124r.
[73] J.P. Perdew, K. Burke, M. Ernzerhof, Generalized Gradient Approximation Made Simple, Phys. Rev. Lett. 77 (1996) 3865–3868. https://doi.org/10.1103/PhysRevLett.77.3865.
[74] J.R. Yates, C.J. Pickard, F. Mauri, Calculation of NMR chemical shifts for extended systems using ultrasoft pseudopotentials, Phys. Rev. B. 76 (2007) 024401. https://doi.org/10.1103/PhysRevB.76.024401.
[75] S. Cadars, R. Guégan, M.N. Garaga, X. Bourrat, L. Le Forestier, F. Fayon, T.V. Huynh, T. Allier, Z. Nour, D. Massiot, New Insights into the Molecular Structures, Compositions, and Cation Distributions in Synthetic and Natural Montmorillonite Clays, Chem. Mater. 24 (2012) 4376–4389. https://doi.org/10.1021/cm302549k.
[76] J.S. Waugh, Sensitivity in Fourier transform NMR spectroscopy of slowly relaxing systems, Journal of Molecular Spectroscopy. 35 (1970) 298–305. https://doi.org/10.1016/0022-2852(70)90205-5.
[77] F.H. Larsen, I. Farnan, 29Si and 17O (Q)CPMG-MAS solid-state NMR experiments as an optimum approach for half-integer nuclei having long T1 relaxation times, Chemical Physics Letters. 357 (2002) 403–408. https://doi.org/10.1016/S0009-2614(02)00520-1.
[78] C.A. Fyfe, K.T. Mueller, H. Grondey, K.C. Wong-Moon, Dipolar dephasing between quadrupolar and spin-12 nuclei. REDOR and TEDOR NMR experiments on VPI-5, Chemical Physics Letters. 199 (1992) 198–204. https://doi.org/10.1016/0009-2614(92)80069-N.
[79] J. Trebosc, B. Hu, J.P. Amoureux, Z. Gan, Through-space R3-HETCOR experiments between spin-1/2 and half-integer quadrupolar nuclei in solid-state NMR, Journal of Magnetic Resonance. 186 (2007) 220–227. https://doi.org/10.1016/j.jmr.2007.02.015.
[80] A. Brinkmann, A.P.M. Kentgens, Proton-Selective 17O−H Distance Measurements in Fast Magic-Angle-Spinning Solid-State NMR Spectroscopy for the Determination of Hydrogen Bond Lengths, J. Am. Chem. Soc. 128 (2006) 14758–14759. https://doi.org/10.1021/ja065415k.
[81] R. Giovine, J. Trébosc, F. Pourpoint, O. Lafon, J.-P. Amoureux, Magnetization transfer from protons to quadrupolar nuclei in solid-state NMR using PRESTO or dipolar-mediated refocused INEPT methods, Journal of Magnetic Resonance. 299 (2019) 109–123. https://doi.org/10.1016/j.jmr.2018.12.016.
[82] J.J. Helmus, C.P. Jaroniec, Nmrglue: an open source Python package for the analysis of multidimensional NMR data, Journal of Biomolecular NMR. 55 (2013) 355–367. https://doi.org/10.1007/s10858-013-9718-x.
[83] C.R. Harris, K.J. Millman, S.J. van der Walt, R. Gommers, P. Virtanen, D. Cournapeau, E. Wieser, J. Taylor, S. Berg, N.J. Smith, R. Kern, M. Picus, S. Hoyer, M.H. van Kerkwijk, M. Brett, A. Haldane, J.F. del Río, M. Wiebe, P. Peterson, P. Gérard-Marchant, K. Sheppard, T. Reddy, W. Weckesser, H. Abbasi, C. Gohlke, T.E. Oliphant, Array programming with NumPy, Nature. 585 (2020) 357–362. https://doi.org/10.1038/s41586-020-2649-2.
[84] D. Massiot, F. Fayon, M. Capron, I. King, S. Le Calvé, B. Alonso, J.-O. Durand, B. Bujoli, Z. Gan, G. Hoatson, Modelling one- and two-dimensional solid-state NMR spectra, Magnetic Resonance in Chemistry. 40 (2002) 70–76. https://doi.org/10.1002/mrc.984.
[85] T. Charpentier, C. Fermon, J. Virlet, Numerical and theoretical analysis of multiquantum magic-angle spinning experiments, J. Chem. Phys. 109 (1998) 3116–3130. https://doi.org/10.1063/1.476903.
[86] F.L. Galeener, G. Lucovsky, Longitudinal Optical Vibrations in Glasses: GeO2 and SiO2, Phys. Rev. Lett. 37 (1976) 1474–1478. https://doi.org/10.1103/PhysRevLett.37.1474.
[87] F.L. Galeener, J.C. Mikkelsen, Vibrational dynamics in O18 -substituted vitreous SiO2, Phys. Rev. B. 23 (1981) 5527–5530. https://doi.org/10.1103/PhysRevB.23.5527.

[88] F.L. Galeener, A.E. Geissberger, Vibrational dynamics in 30Si-substituted vitreous SiO2, Physical Review B. 27 (1983) 6199–6204.
[89] R.A. Barrio, F.L. Galeener, E. Martínez, R.J. Elliott, Regular ring dynamics in AX 2 tetrahedral glasses, Phys. Rev. B. 48 (1993) 15672–15689. https://doi.org/10.1103/PhysRevB.48.15672.
[90] F.L. Galeener, Planar rings in glasses, Solid State Communications. 44 (1982) 1037–1040.
[91] P.F. Mcmillan, B.T. Poe, P. Gillet, B. Reynard, A study of SiO2 glass and supercooled liquid to 1950 K via high-temperature Raman spectroscopy, Geochimica et Cosmochimica Acta. 58 (1994) 3653–3664.
[92] R.H. Stolen, G.E. Walrafen, Water and its relation to broken bond defects in fused silica, The Journal of Chemical Physics. 64 (1976) 2623–2631. https://doi.org/10.1063/1.432516.
[93] H. Behrens, J. Roux, D.R. Neuville, M. Siemann, Quantification of dissolved H2O in silicate glasses using confocal microRaman spectroscopy, Chemical Geology. 229 (2006) 96–112. https://doi.org/10.1016/j.chemgeo.2006.01.014.
[94] T. Beuvier, M. Richard-Plouet, L. Brohan, Accurate Methods for Quantifying the Relative Ratio of Anatase and TiO_2 (B) Nanoparticles, J. Phys. Chem. C. 113 (2009) 13703–13706. https://doi.org/10.1021/jp903755p.
[95] I.I. Kornilov, V.V. Vavilova, L.E. Fykin, R.P. Ozerov, S.P. Solowiev, V.P. Smirnov, Neutron diffraction investigation of ordered structures in the titanium-oxygen system, Metallurgical Transactions. 1 (1970) 2569. https://doi.org/10.1007/BF03038386.
[96] I. Farnan, P.J. Grandinetti, J.H. Baltisberger, J.F. Stebbins, U. Werner, M.A. Eastman, A. Pines, Quantification of the disorder in network-modified silicate glasses, Nature. 358 (1992) 31–35. https://doi.org/10.1038/358031a0.
[97] S. Wang, J.F. Stebbins, Multiple-Quantum Magic-Angle Spinning 17O NMR Studies of Borate, Borosilicate, and Boroaluminate Glasses, Journal of the American Ceramic Society. 82 (1999) 1519–1528. https://doi.org/10.1111/j.1151-2916.1999.tb01950.x.
[98] F. Angeli, T. Charpentier, S. Gin, J.C. Petit, 17O 3Q-MAS NMR characterization of a sodium aluminoborosilicate glass and its alteration gel, Chemical Physics Letters. 341 (2001) 23–28. https://doi.org/10.1016/S0009-2614(01)00423-7.
[99] F. Angeli, T. Charpentier, M. Gaillard, P. Jollivet, Influence of zirconium on the structure of pristine and leached soda-lime borosilicate glasses: Towards a quantitative approach by 17O MQMAS NMR, Journal of Non-Crystalline Solids. 354 (2008) 3713–3722. https://doi.org/10.1016/j.jnoncrysol.2008.03.046.
[100] K.J.D. MacKenzie, M.E. Smith, eds., Multinuclear solid-state NMR of inorganic materials, Pergamon, Amsterdam, 2002.
[101] S.K. Lee, J.F. Stebbins, Nature of Cation Mixing and Ordering in Na-Ca Silicate Glasses and Melts, J. Phys. Chem. B. 107 (2003) 3141–3148. https://doi.org/10.1021/jp027489y.
[102] T.M. Clark, P.J. Grandinetti, P. Florian, J.F. Stebbins, Correlated structural distributions in silica glass, Phys. Rev. B. 70 (2004) 064202. https://doi.org/10.1103/PhysRevB.70.064202.
[103] N.M. Trease, T.M. Clark, P.J. Grandinetti, J.F. Stebbins, S. Sen, Bond length-bond angle correlation in densified silica—Results from 17O NMR spectroscopy, J. Chem. Phys. 146 (2017) 184505. https://doi.org/10.1063/1.4983041.
[104] E. Scolan, C. Magnenet, D. Massiot, C. Sanchez, Surface and bulk characterisation of titanium–oxo clusters and nanosized titania particles through 17O solid state NMR, J. Mater. Chem. 9 (1999) 2467–2474. https://doi.org/10.1039/A903714D.
[105] R.D. Shannon, Revised effective ionic radii and systematic studies of interatomic distances in halides and chalcogenides, Acta Crystallographica Section A. 32 (1976) 751–767. https://doi.org/10.1107/S0567739476001551.
[106] X. Cong, R.J. Kirkpatrick, 17O MAS NMR Investigation of the Structure of Calcium Silicate Hydrate Gel, Journal of the American Ceramic Society. 79 (1996) 1585–1592. https://doi.org/10.1111/j.1151-2916.1996.tb08768.x.

[107] X. Cong, R.J. Kirkpatrick, 29Si and 17O NMR investigation of the structure of some crystalline calcium silicate hydrates, Advanced Cement Based Materials. 3 (1996) 133–143. https://doi.org/10.1016/S1065-7355(96)90045-0.
[108] M.F. Best, R.A. Condrate, A raman study of TiO2-SiO2 glasses prepared by sol-gel processes, J Mater Sci Lett. 4 (1985) 994–998. https://doi.org/10.1007/BF00721102.
[109] K.L. Walther, A. Wokaun, B.E. Handy, A. Baiker, TiO2/SiO2 mixed oxide catalysts prepared by sol—gel techniques. Characterization by solid state CP/MAS spectroscopy, Journal of Non-Crystalline Solids. 134 (1991) 47–57. https://doi.org/10.1016/0022-3093(91)90010-4.
[110] J.P. Rainho, J. Rocha, L.D. Carlos, R.M. Almeida, ^{29} Si nuclear-magnetic-resonance and vibrational spectroscopy studies of SiO_2 –TiO_2 powders prepared by the sol-gel process, J. Mater. Res. 16 (2001) 2369–2376. https://doi.org/10.1557/JMR.2001.0325.
[111] M.J. Davis, P.D. Ihinger, A.C. Lasaga, Influence of water on nucleation kinetics in silicate melt, Journal of Non-Crystalline Solids. 219 (1997) 62–69. https://doi.org/10.1016/S0022-3093(97)00252-4.
[112] J. Deubener, R. Müller, H. Behrens, G. Heide, Water and the glass transition temperature of silicate melts, Journal of Non-Crystalline Solids. 330 (2003) 268–273. https://doi.org/10.1016/S0022-3093(03)00472-1.
[113] P. Del Gaudio, H. Behrens, J. Deubener, Viscosity and glass transition temperature of hydrous float glass, Journal of Non-Crystalline Solids. 353 (2007) 223–236. https://doi.org/10.1016/j.jnoncrysol.2006.11.009.
[114] E.D. Zanotto, The formation of unusual glasses by sol-gel processing, Journal of Non-Crystalline Solids. 147–148 (1992) 820–823. https://doi.org/10.1016/S0022-3093(05)80723-9.
[115] E.D. Zanotto, J.C. Mauro, The glassy state of matter: Its definition and ultimate fate, Journal of Non-Crystalline Solids. 471 (2017) 490–495. https://doi.org/10.1016/j.jnoncrysol.2017.05.019.
[116] J.F. White, J. Lee, O. Hessling, B. Glaser, Reactions Between Liquid CaO-SiO2 Slags and Graphite Substrates, Metallurgical and Materials Transactions B. 48 (2017) 506–515. https://doi.org/10.1007/s11663-016-0788-5.
[117] V.O. Sokolov, V.G. Plotnichenko, E.M. Dianov, Quantum-chemical modeling of titanium centers in titanosilicate glass, Inorganic Materials. 42 (2006) 1273–1288. https://doi.org/10.1134/S0020168506110173.
[118] G.A. Tompsett, G.A. Bowmaker, R.P. Cooney, J.B. Metson, K.A. Rodgers, J.M. Seakins, The Raman spectrum of brookite, TiO2 (Pbca, Z = 8), J. Raman Spectrosc. 26 (1995) 57–62. https://doi.org/10.1002/jrs.1250260110.
[119] H.L. Ma, J.Y. Yang, Y. Dai, Y.B. Zhang, B. Lu, G.H. Ma, Raman study of phase transformation of TiO2 rutile single crystal irradiated by infrared femtosecond laser, Applied Surface Science. (2007) 4.
[120] G. Urbain, Y. Bottinga, P. Richet, Viscosity of liquid silica, silicates and alumino-silicates, Geochimica et Cosmochimica Acta. 46 (1982) 1061–1072. https://doi.org/10.1016/0016-7037(82)90059-X.

Research data

Research Data associated with this article can be accessed on the repository “www.zenodo.org” using the following link: https://doi.org/10.5281/zenodo.6513443 .